

Energy & Environmental Science

Accepted Manuscript



This is an *Accepted Manuscript*, which has been through the Royal Society of Chemistry peer review process and has been accepted for publication.

Accepted Manuscripts are published online shortly after acceptance, before technical editing, formatting and proof reading. Using this free service, authors can make their results available to the community, in citable form, before we publish the edited article. We will replace this *Accepted Manuscript* with the edited and formatted *Advance Article* as soon as it is available.

You can find more information about *Accepted Manuscripts* in the [Information for Authors](#).

Please note that technical editing may introduce minor changes to the text and/or graphics, which may alter content. The journal's standard [Terms & Conditions](#) and the [Ethical guidelines](#) still apply. In no event shall the Royal Society of Chemistry be held responsible for any errors or omissions in this *Accepted Manuscript* or any consequences arising from the use of any information it contains.

An Overview on Metal Oxide Materials as Electrocatalysts and Supports for Polymer Electrolyte Fuel Cells

Zhonghua Zhang^{a*}, Jie Liu^a, Junjie Gu^a, Liang Su^b, Lifeng Cheng^c

^a Department of Mechanical and Aerospace Engineering, Carleton University, Ottawa, ON, Canada, K1S 5B6.

^b Department of Chemical Engineering, Massachusetts Institute of Technology, Cambridge, MA 02139, USA.

^c Département de Chimie, Université de Montréal, Montréal, QC, Canada, H3T 1J4.

E-mail: zhonghua.zhang@carleton.ca

Abstract

Polymer electrolyte fuel cells (PEFCs) are promising power sources in portable and transportation applications because of their high-energy density, low-operating temperature and easiness in transportation and storage. However, high cost, low activity and short durability of electrocatalysts are restraining the commercialization of PEFCs. Metal oxides have abundant sources, low price, high chemical and electrochemical stability, abundant hydroxyl groups on the surface, and strong interaction with metal nanoparticles, and thus are promising to reduce the present problems in PEFCs. In this review, binary metal oxides such as titanium oxide, tungsten oxide, molybdenum oxide, ruthenium oxide, tin oxide, cerium oxide and manganese oxide, and multi-component perovskite oxides are chosen based on the selection criteria of metal oxides and introduced as independent electrocatalysts, co-catalysts and supports for various anode

oxidation and cathode reduction reactions in PEFCs. The effects of compositions, morphologies, doping and mixing of metal oxides on their electrocatalytic performance for PEFCs have also been summarized. Finally, several most promising metal oxides and possible research trends on metal oxides are recommended for future PEFCs.

Keywords: polymer electrolyte fuel cells, metal oxides, titanium oxides, tungsten oxides, tin oxides, perovskite oxides.

Table of Contents

1. Introduction	1
2. Selection criteria	4
3. Research progress of metal oxides in PEFCs	5
3.1. Titanium oxides (TiO_x)	6
3.1.1. Stoichiometric TiO_2	6
3.1.2. Sub-stoichiometric $\text{Ti}_n\text{O}_{2n-1}$	8
3.1.3. Doped TiO_2	9
3.1.4. TiO_2/C or carbon nanotubes (CNT) mixture	12
3.1.5. Morphological influence of TiO_2	13
3.1.6. Photo-electro-catalysis of TiO_2 for PEFCs	15
3.2. Tungsten oxides (WO_x)	17
3.2.1. WO_x	18
3.2.2. Doped WO_3	19
3.2.3. WO_3/C or CNT mixture	19
3.2.4. Morphological influence of WO_3	21
3.3. Molybdenum oxides (MoO_x)	22
3.3.1. MoO_2	23
3.3.2. MoO_3	23
3.3.3. MoO_x	24

3.3.4.	H_xMoO_3	26
3.4.	Ruthenium oxides (RuO_x).....	26
3.4.1.	Ruthenium dioxide (RuO_2).....	27
3.4.2.	Hydrous ruthenium oxide (RuO_xH_y or $RuO_2 \cdot xH_2O$).....	28
3.4.3.	RuO_x -based composite oxides.....	30
3.4.4.	Morphological influence of RuO_2	30
3.5.	Tin oxides (SnO_x).....	31
3.5.1.	SnO_2	32
3.5.2.	Doped SnO_2	33
3.5.3.	Morphological influence of SnO_2	34
3.6.	Cerium oxide (CeO_2).....	35
3.6.1.	CeO_2	36
3.6.2.	Doped CeO_2	38
3.7.	Manganese oxides (MnO_x).....	39
3.7.1.	MnO_2	40
3.7.2.	$MnOOH$	41
3.7.3.	Mn_2O_3	42
3.7.4.	Mn_3O_4	42
3.7.5.	MnO	43
3.7.6.	Morphological influence of MnO_x	43

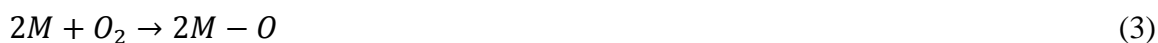
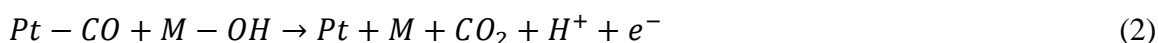
3.8. Perovskite oxide (ABO_3).....	45
3.8.1. Structure and property.....	45
3.8.2. Application in alkaline PEFCs.....	45
4. Conclusions and Perspectives.....	47
References.....	51

1. Introduction

Polymer electrolyte fuel cells (PEFCs) have attracted increased interests as promising power sources in portable and transportation applications because of their high energy density (resulting from employed fuels with high energy density), low operating temperature and easiness in transportation and storage.¹ However, as far as PEFC catalysts are concerned, there are some problems to solve before their wide commercialization: cost, performance and durability. The most frequently used electrocatalysts are Pt or Pt-based materials. It is well known that Pt is expensive and limited because of its low content in the earth crust. Considering its application in fuel cell vehicles, the natural resource of Pt is insufficient. As for performance, even if Pt is used as a cathode electrocatalyst in the present PEFCs, its catalytic activity for the oxygen reduction reaction is still insufficient to obtain the required efficiency.² Therefore, many attempts such as preparation of fine nanocatalysts, an alloying with transition metals, and high dispersion of Pt particles on a support with high specific surface area, have been made to reduce Pt usage and thus cost, and improve its performance for PEFCs. Another important issue is long-term durability of electrocatalysts. During long time running of PEFCs, the agglomeration of metal nanoparticles and electrochemical corrosion of supports lead to the degradation of catalysts.³ The agglomeration of metal nanoparticles can be reduced by choosing a support which has strong interaction with metal. The corrosion of the common support carbon black occurs at voltages above ~ 0.9 V, which can cause metal nanoparticles to be released from the support and agglomerate, limiting the catalyst surface area that can be accessed by oxygen or fuel molecules, and thus leads to the degradation of overall fuel cell efficiency. Therefore, it is necessary for

PEFCs' long time running to find a stable support in electrochemical and strong acid/alkaline environment. For example, carbon nitride instead of carbon black has been employed as the support of noble metal nanocatalysts to enhance the durability and corrosion-tolerance of the catalysts.⁴⁻⁷

The common reactions in PEFCs include hydrogen oxidation reaction (HOR), methanol oxidation reaction (MOR), ethanol oxidation reaction (EOR) and formic acid oxidation reaction (FAOR) at anode, and oxygen reduction reaction (ORR) at cathode. Electronic effect and bifunctional mechanism of Pt-based catalysts are often involved in HOR, MOR, EOR and FAOR. The presence of an electronic effect leads to the shift of Pt d-band center and thus weakens the bond strength of intermediates adsorbed on the catalysts.⁸ The bifunctional mechanism of Pt and another metal can remove strong adsorbed intermediate CO effectively as shown in Eqs. 1 and 2.⁹ ORR at the cathode occurs principally by the direct 4-electron pathway on Pt-based electrocatalysts, which involves an initial dissociative chemisorption of O₂ (Eq. 3) and the subsequent reduction of adsorbed oxygen atoms to water (Eq. 4).¹⁰



Metal oxides based on non-noble metals because of their abundant sources, low price and environmental friendliness have wide applications in various fields. They have important characteristics of their potential application in PEFCs: 1) they have much higher corrosion resistance in electrochemical environment of PEFCs compared with carbon

because metals in metal oxides exist as a high oxidative state and are difficult to further lose electrons to be oxidized; 2) they as co-catalysts or supports often have strong interactions with metal catalyst particles. The strong interactions could prevent the agglomeration of metal particles and maintain small metal particle size.¹¹ It could also produce an electronic effect and modify the catalytic property of metal catalysts; 3) they have abundant hydroxyl groups on their surface, which could function as co-catalysts of noble metal catalysts based on a bifunctional mechanism.⁸ Because of their outstanding advantages, metal oxides have been used as independent electrocatalysts, co-catalysts and supports for PEFCs in aqueous acidic and alkaline electrolytes.

Many reviews about fuel cell electrocatalysts focused on Pt-based and non-Pt metal catalysts.^{2,12} There are few reviews about metal oxides in PEFCs.¹³ In this review, we first introduced selection criteria of metal oxides and chose binary metal oxides such as titanium oxide (TiO_x), tungsten oxide (WO_x), molybdenum oxide (MoO_x), ruthenium oxide (RuO_x), tin oxide (SnO_x), cerium oxide (CeO_2) and manganese oxide (MnO_x), and multi-component metal oxides perovskite oxides (ABO_3) for PEFCs. Then we investigated the catalytic performance of these metal oxides as independent electrocatalysts (principally MnO_x and perovskites for ORR in alkaline electrolyte) and as co-catalysts and supports for various PEFC reactions in aqueous acidic and alkaline electrolytes (TiO_x , WO_x , MoO_x , RuO_x , SnO_x and CeO_2 for HOR, MOR, EOR, FAOR and ORR). Meanwhile, we also summarized the effects of compositions, doping, mixing and morphologies of metal oxides on their electrocatalytic performance for PEFCs. Finally, we displayed several most promising metal oxides and recommended possible research directions on metal oxides for PEFCs in aqueous acidic and alkaline electrolytes.

2. Selection criteria

In searching for suitable metal oxide materials for PEFCs, several important requirements need to be considered by researchers.

- 1) High stability in acidic media for acidic fuel cells or in alkaline media for alkaline fuel cells – The prerequisite for the application of metal oxides in PEFCs is that metal oxides cannot dissolve in acidic media when used in acidic fuel cells or in alkaline media when used in alkaline fuel cells. For example, titanium oxide, tungsten oxide, molybdenum oxide and ruthenium oxide, etc. are stable in acidic media, while manganese oxide and perovskite oxides are stable in alkaline media. However, some amphoteric metal oxides such as Al_2O_3 , V_2O_5 and ZnO cannot be used in both media, while many alkaline metal oxides such as MgO , CaO and CuO should be avoided in acidic media.
- 2) High resistance against electrochemical corrosion: Metal oxides should be electrochemically stable in the working conditions of PEFCs, or metal nanoparticles supported on them will peel from them and agglomerate, leading to the degradation of catalytic performance. For example, there was no oxidation peak observed between 0 and 2.0 V vs. NHE in 1 M sulfuric acid for Magnéli phase titanium oxides.¹⁴
- 3) Good electronic conductivity: Metal oxides should be conductive enough to potentially allow for ultralow Pt loadings on the surface. Doping of other metal ions can increase the conductivity of an insulating oxide, while mixing with carbon black or carbon nanotubes (CNT) to form oxide-carbon nanocomposites can improve their electronic conductivity markedly.

- 4) Good proton conductivity: Metal oxides with good proton conductivity ease the transfer of protons and thus electrocatalysis of HOR and ORR. For example, WO_3 and MoO_3 can form hydrogen tungsten/molybdenum bronzes (H_xWO_3 and H_xMoO_3) and markedly enhance the electronic and proton conductivity of metal oxides.
- 5) High specific surface area: High specific surface area can accomplish fine dispersion and high utilization of noble metal nanoparticles on metal oxides. Supporting metal oxides nanoparticles on carbon materials with a large specific surface area as composite supports can also realize this requirement.
- 6) Proper porosity: Proper porosity of metal oxides is favorable for mass transfer of liquid fuels or oxygen gas and the minimization of water flooding in electrodes.
- 7) Compatibility with electrodes: Metal oxides should bond well with noble metal nanoparticles to maintain adhesion and a conductive link to noble metal nanoparticles and to form a good three-phase boundary.

In view of the above selection criteria, we chose the following metal oxides to show as successful examples in PEFCs: binary metal oxides – titanium oxides (TiO_x), tungsten oxides (WO_x), molybdenum oxides (MoO_x), ruthenium oxides (RuO_x), tin oxide (SnO_x), cerium oxide (CeO_2) and manganese oxide (MnO_x); multi-component metal oxides – perovskite oxides (ABO_3).

3. Research progress of metal oxides in PEFCs

3.1. Titanium oxides (TiO_x)

Titanium oxides have been widely applied in photoelectric and electric fields since their use by Fujishima and Honda for electrochemical photolysis of water.¹⁵ They have been considered potential supports for PEFCs because of their stability in fuel cell operation atmosphere, low cost, non-toxicity, commercial availability, and the ease to control size and structure. A big advantage is the presence of a strong interaction between titanium oxides and metal nanoparticles,¹⁶ which could avoid the agglomeration of metal particles, disperse metal atoms in the clusters, and change the electronic property of metal nanocatalysts.

3.1.1. Stoichiometric TiO_2

Early in 1980's and 1990's, TiO_2 was used for the reduction of oxygen in acidic and alkaline solution.^{17, 18} The majority of the ORR on TiO_2 was found to proceed via a 4-electron pathway. Later, Kim et al. prepared TiO_2 catalyst by heat-treating Ti sheets at 900°C and found that TiO_2 as a non-Pt catalyst exhibits an onset potential of ca. 0.65V vs. NHE for ORR.¹⁹ The catalytic activity of Ti oxides increases with the (110) plane of the rutile TiO_2 and the work function. Hepel et al. applied quantum mechanical calculations to the study on the support-catalyst cluster interactions and surface diffusivity of adsorbed intermediates on bimetallic catalysts supported on nanoporous TiO_2 .²⁰ Figure 1 shows the effect of addition of one Pt atom to a $(\text{TiO}_2)_6$ surface on electronic properties of the system. When there is no Pt- TiO_2 bond formation (Figure 1a), a small charge transferred from TiO_2 to Pt leads to slight lowering of the HOMO energy level. When a Pt atom forms bonds with O atoms of TiO_2 (Figure 1b), the charge transfers from Pt to

TiO₂, which results in dramatic changes in both HOMO and LUMO levels. When a Pt atom forms bonds with Ti atoms of TiO₂ (Figure 1c), the electron cloud even spreads on all the surface atoms. The strong metal-support interaction lowers the activation energy for CO_{ad} surface mobility, and leads to a more facile 2D diffusion of CO_{ad} from Pt sites to Ru and TiO₂, and thus a lower poisoning effect for PtRu on a TiO₂ support compared with unsupported PtRu or bare Pt catalysts. Gustavsson et al. deposited directly Pt and TiO₂ films on Nafion membrane by a thermal evaporation technique and found that a thin layer of TiO₂ between Pt and Nafion increases the ORR performance compared with a Pt film deposited directly on Nafion.²¹ The improvement is because of the better dispersion of Pt on TiO₂ and substantial proton conduction through the thin TiO₂ layer. Rajalakshmi et al. found that Pt/TiO₂ has better thermal stability and electrochemical activity than Pt/C.²² The presence of TiO₂ in Pt was recommended to avoid the agglomeration of Pt particles, effectively disperse the Pt atoms in the clusters, and provide thermal and oxidation stability against corrosion. Huang et al. prepared Pt-Ir/TiO₂ catalysts and investigated their catalytic activity for ORR.²³ The round-trip energy conversion efficiency of the supported Pt-Ir/TiO₂ (42%) is significantly higher than that of unsupported Pt-Ir black (30%). Although TiO₂ as support or catalyst exhibits some catalytic performance, its low electronic conductivity and surface area still restrain its widespread applications in PEFCs. Such problems have been reduced by the change of composition and morphology of TiO₂ discussed as follows.

3.1.2. Sub-stoichiometric $\text{Ti}_n\text{O}_{2n-1}$

For electrochemical applications such as PEFCs, the increase of electronic conductivity in TiO_2 is necessarily required. One of the methods to improve the electronic conductivity of TiO_2 is to reduce pure titanium oxide and produce oxygen vacancies to obtain sub-stoichiometric titanium oxides. The presence of oxygen vacancies and titanium interstitials can lower the band gap and thus increase the electronic conductivity of titanium oxides. Sub-stoichiometric titanium oxides known as Magnéti phase have a general formula of $\text{Ti}_n\text{O}_{2n-1}$ ($4 < n < 10$) and exhibit a high conductivity comparable to that of graphite.²⁴ For example, the conductivity of Ti_4O_7 phase even reaches ca. 10^3 S cm^{-1} at room temperature.²⁵ In addition, there was no oxidation peaks observed between 0 and 2.0 V vs. NHE in 1 M sulfuric acid for Magnéti phase titanium oxides.¹⁴ High conductivity and strong oxidation resistance make Magnéti phase titanium oxides possible as PEFC catalyst support materials.

Since Chen et al. reported Pt-Ru-Ir catalysts deposited on Ebonex (several sub-oxides of titanium oxide, principally Ti_4O_7 and Ti_5O_9) and Ti_4O_7 as bifunctional oxygen reduction/water oxidation catalysts,²⁶ Ioroi group has carried out a series of work about Ti_4O_7 as a catalyst support for fuel cell applications. They prepared Ti_4O_7 by reducing TiO_2 powder at high temperature under H_2 atmosphere and found that Ti_4O_7 has much higher onset oxidation potential (ca. 1.8 V) than Vulcan XC-72 (ca. 0.9 V), and be very stable under PEFC operating conditions.²⁷ The Pt nanocatalysts supported on Ti_4O_7 exhibit the similar specific activity for both HOR and ORR to the Pt/C catalyst. They further investigated the effects of high-potential holding and cycling on the electrochemical activity and stability of Pt/ Ti_4O_7 catalyst.^{28, 29} The Pt/ Ti_4O_7 catalyst is

quite stable against high potential up to 1.5 V. When Pt/Ti₄O₇ is used as the cathode in pure H₂/O₂ fuel cell, there is no degradation in voltage even after the operation at 300 mA cm⁻² for 350 hours. To increase the surface area of titanium oxide support, Ioroi et al. developed a new pulsed UV laser irradiation method to obtain nanometric Magnéli phase TiO_x with a specific surface area of more than 20 m² g⁻¹.^{30, 31} The resultant Pt-TiO_x and Pt-Ti/TiO_x catalysts exhibit 2-fold higher specific activity for ORR than Pt/Vulcan XC72 after the cyclic tests sweeping from 0.05 to 1.0 V at a scan rate of 10 mV s⁻¹ in 0.1 M HClO₄ at 25°C by rotating disk electrode technique. As shown in Figure 2, they retain their initial electrochemical active area even after 10,000 cycles between 1.0 and 1.5 V. Recently, Zhang et al. also developed Ti₄O₇ supported Ru@Pt core-shell catalyst by pyrolysis followed by microwave irradiation.³² The catalyst exhibits a higher CO-tolerance ability for H₂ oxidation with CO at various concentrations than PtRu/C alloy catalyst.

Obviously, sub-stoichiometric titanium oxides show obvious co-catalytic performance for Pt in PEFCs. However, it must be mentioned that they tend to be oxidized to stoichiometric TiO₂ in long-time cell operation, which causes a degradation of electronic conductivity and thus electrocatalytic performance. Therefore, how to enhance the durability of sub-stoichiometric titanium oxides in long-time cell operation is still a challenge.

3.1.3. Doped TiO₂

Another method to improve the electronic conductivity of TiO₂ is doping with other metals. The most studied material is Nb-doped TiO₂ which has an electronic conductivity

of $0.2 - 1.5 \text{ S cm}^{-1}$.²⁶ When TiO_2 is doped with Nb, the charge compensation for Nb^{5+} substituting Ti^{4+} is achieved either by the creation of one Ti cation vacancy per four Nb atoms or by the stoichiometric reduction of Ti^{4+} to Ti^{3+} . Chen et al. attempted to employ $\text{Nb}_{0.1}\text{Ti}_{0.9}\text{O}_2$ as the support of PtRuIr catalysts and found that $\text{Nb}_{0.1}\text{Ti}_{0.9}\text{O}_2$ has a wide potential window ranging from -0.4 to 2 V vs. NHE and exhibits even more excellent stability than Ebonex and Ti_4O_7 .²⁶ Garca et al. prepared $\text{Nb}_{0.1}\text{Ti}_{0.9}\text{O}_2$ with BET surface area of $136 \text{ m}^2 \text{ g}^{-1}$ by a sol-gel method and deposited PtRu on the support by LiBH_4 reduction in tetrahydrofuran.³³ The PtRu/ $\text{Nb}_{0.1}\text{Ti}_{0.9}\text{O}_2$ catalyst exhibits 6% higher mass activity and 100% higher specific activity than PtRu/C. The membrane electrode assembly (MEA) with PtRu/ $\text{Nb}_{0.1}\text{Ti}_{0.9}\text{O}_2$ has 46% higher mass activity than an equivalent E-TEK MEA. Park et al. prepared Nb-doped TiO_2 with particle size of $\sim 10 \text{ nm}$ by a hydrothermal method and supported Pt nanoparticles on the support by a borohydride reduction method.³⁴ As shown in Figure 3, the resultant Pt/Nb- TiO_2 catalyst exhibits higher onset potentials (1.0 V) and mass activity of Pt ($235.3 \text{ mA mg}^{-1}@0.8 \text{ V}$) for ORR than those (0.9 V and $58.8 \text{ mA mg}^{-1}@0.8 \text{ V}$) of Pt/Vulcan XC-72. The improvement in ORR performance is attributed to both the good dispersion of Pt nanoparticles on Nb- TiO_2 support, and the interaction between oxide support and metal catalyst as analyzed from the XANES spectra of Pt L edge. Fuentes et al. synthesized Nb-doped TiO_2 using two sol-gel procedures and deposited PtRu on the support.³⁵ The PtRu/Nb- TiO_2 catalyst exhibits a high activity for MOR comparable to the commercial PtRu/C catalyst. Chhina et al. investigated the activity and stability of Pt supported on 10 mol% Nb-doped TiO_2 in PEFCs and found that the catalyst has a significantly higher stability than commercial Pt/C.³⁶ Pt surface area is still stable at Pt/Nb- TiO_2 even after holding at 1.4 V for 60 h,

while it has a significant drop at Pt/C after holding at 1.4 V for 20 h. Gojković et al. synthesized 0.5% Nb-doped TiO₂ with BET surface area of 72 m² g⁻¹ by an acid-catalyzed sol-gel method and employed it as the support for Pt and PtRu catalyst.³⁷ The resultant Pt/Nb-TiO₂ and PtRu/Nb-TiO₂ catalysts exhibit the comparable catalytic activity to those supported on XC-72 with a high surface area. Besides Nb as a dopant of TiO₂, Haas reported Ru-doped TiO₂ by a sol-gel method and deposited Pt nanoparticles on the support.³⁸ The conductivity of the support increases with Ru mole fraction. The Pt/Ru_xTi_{1-x}O₂ catalyst has an active Pt surface area comparable to commercial catalysts on carbon support. Ho et al. also reported Mo-doped TiO₂ as the support of Pt nanocatalysts for ORR.³⁹ As shown in the Pt L_{III}-edge XANES spectrum of Figure 4, the Pt/Ti_{0.7}Mo_{0.3}O₂ catalyst has the lowest white line intensity, that is, the least Pt d-band vacancy. The dramatic decrease in the d-band vacancy of Pt means that there is the largest electron donation from the Ti_{0.7}Mo_{0.3}O₂ support to Pt because of the strong metal-support interaction (SMSI). The SMSI leads to not only 7 and 2.6 fold higher activity of Pt/Ti_{0.7}Mo_{0.3}O₂ than those of commercial Pt/C and PtCo/C catalysts, but also its high stability during potential cycling.

Nb doping can improve the electronic conductivity of TiO₂ by creating more Ti vacancies, while Mo doping can donate more electrons from TiO₂ support to Pt by a strong metal-support interaction. These results give us some inspiration: if doping of other metal ions can create more Ti vacancies or donate more electrons to Pt, it is possible to develop highly co-catalytic TiO₂ by doping.

3.1.4. TiO₂/C or carbon nanotubes (CNT) mixture

One simple and general method to improve the electronic conductivity and surface area of TiO₂ is to mix carbon or CNT with TiO₂ to form a composite support.⁴⁰⁻⁴² Chen et al. prepared Pt-Ru-Ti/C catalyst by introducing TiO₂ to the Pt-Ru matrix and found that the catalyst has better catalytic activity for MOR than the PtRu/C catalysts.⁴³ They found the presence of TiO₂ can dramatically decrease the grain size of the catalyst to about 1-2 nm and markedly improve the intra-particle distribution. They also demonstrated a multi-scale model of the Pt-Ru-Ti/C catalyst based on extended X-ray absorption fine spectra (EXAFS) analysis. As shown in Figure 5, the PtRu/C catalysts from Johnson-Matthey (West Chester, Pennsylvania, USA), E-TEK (De Nora North America, Inc., New Jersey, USA) and in-house preparations show a structure with a Pt-rich core surrounded by a Ru-rich shell. However, there is no obvious segregation of Pt and Ru atoms in the Pt-Ru-Ti/C catalyst, which shows the role of TiO₂ in enhancing the dispersion of the Pt and Ru atoms in the catalyst clusters and improving the intra-particle dispersion. Muhamad et al. reported that TiO₂-modified Pd/C catalyst shows the high activity for CO/H₂ fuels comparable to the Pt/C catalyst.⁴⁴ The addition of TiO₂ increases not only the dispersion of metal particles and thus electrochemical active surface area, but also the CO tolerance. Selvarani et al. explored the Pt-TiO₂/C catalysts with various Pt-Ti atomic ratios for ORR and found the Pt-TiO₂/C heat-treated at 750°C with an atomic ratio of 2:1 for Pt and Ti shows enhanced methanol tolerance while maintaining high catalytic activity.⁴⁵ The DMFC with a Pt-TiO₂/C cathode exhibits an enhanced peak power density of 180 mW cm⁻² compared with 80 mW cm⁻² for the DMFC with Pt/C. Wang and Qu synthesized Pd nanoparticles supported on TiO₂-C composite supports and investigated their catalytic

performance for FAOR.^{46, 47} They found that the addition of TiO₂ significantly increases catalytic activity and stability of Pd for FAOR due to the outstanding oxidation and acid corrosion resistance of TiO₂.

CNTs because of their good conductivity, high specific surface area and excellent stability have also been mixed with TiO₂ as the composite support for PEFCs. Song et al. coated a thin layer of amorphous TiO₂ on CNTs by a sol-gel method and prepared Pt nanoparticles on the composite support by an ethylene glycol reduction method.⁴⁸ The Pt-TiO₂/CNTs catalyst exhibits higher electrocatalytic activity and CO tolerance for EOR than the commercial Pt/C and Pt/CNTs. Akalework et al. synthesized multiwalled carbon nanotube supported ultrathin TiO₂ films (MWCNT@UT-TiO₂) using a modified sol-gel method and deposited Pt on the composite support by a formic acid reduction method.⁴⁹ The resultant Pt-MWCNT@UT-TiO₂ exhibits better catalytic activity and durability than Pt/MWCNT and Pt/C. As shown in Figure 6, there are more electrons transferred from MWCNT@UT-TiO₂ to Pt than those from MWCNT to Pt, which shows that the improvement in catalytic performance results from the stronger metal-support interaction between MWCNT@UT-TiO₂ support and Pt nanoparticles.

3.1.5. Morphological influence of TiO₂

The morphology of TiO₂ supports has a marked influence on their physical properties and electrochemical performance. For example, oriented polycrystalline titania nanotubes offer the advantages of directed electron transfer and are expected to have higher electron mobility compared with sintered nanoparticle films.⁵⁰

The most studied morphology of TiO_2 is nanotubes and nanotube arrays as PEFC supports. Song et al. merely mixed the home-made TiO_2 nanotubes with the commercial Pt/C catalyst.⁵¹ The resultant Pt/C- TiO_2 nanotubes have higher catalytic activity and stability for EOR than the Pt/C- TiO_2 powder and Pt/C catalysts, and can promote the oxidation of pre-adsorbed CO at lower potential. They further found that the structural water in TiO_2 nanotubes is favorable for enhancing the poison resistance ability of catalysts.⁵² The Au and Pt nanocatalysts supported on TiO_2 nanotubes were found to have high ORR activity and stability.^{53, 54} Maiyalagan and Jiang prepared Pt/ TiO_2 nanotubes and Pt(5%)-Ni(10%)- TiO_2 nanotube(10%)/C, respectively.^{55, 56} The catalysts exhibit better catalytic performance for MOR than the commercial E-TEK catalyst. Rettew et al. prepared Pt nanocatalysts supported on TiO_2 nanotube arrays by spontaneous growth and galvanic replacement of a Cu precursor layer.⁵⁷ As shown in XPS spectra of Figure 7, Pt exists in a cationic state for the spontaneously deposited Pt and the Pt after a 1-min Cu treatment, while Pt exists in the form of metallic state for the sample modified with a 5-min Cu deposition, indicating that by increasing the thickness of the pre-deposited Cu layer, the interaction between Pt metal and TiO_2 support is increased and the surface Pt is rendered metallic rather than cationic, which further increases the activity of Pt for MOR. Besides nanotubes, nanorods, nanofibers and nanosheets of TiO_2 have also been used as the supports for PEFCs. Guo et al. prepared Pt nanocatalyst supported on porous anatase TiO_2 nanorods.⁵⁸ The catalyst exhibits excellent electrocatalytic activity and stability for MOR, attributed to the excellent dispersion of Pt nanoparticles and the high CO tolerance of TiO_2 support. He et al. deposited Pt nanoparticles onto TiO_2 nanorod arrays on a Ti foil and found that the Pt/ TiO_2 /Ti catalyst exhibits much higher catalytic activity and

stability for EOR in both acidic and alkaline media than Pt/C and Pt/Ti catalysts,⁵⁹ indicating that this improvement results from much larger surface area because of the 3D structure of TiO₂ support for well-dispersed Pt nanoparticles. Long et al. prepared TiO₂ nanofibers by an electrospinning method, then coated Pt nanoparticles on the TiO₂ nanofibers by an intermittent microwave irradiation technique.⁶⁰ The resultant Pt/TiO₂ nanofiber composites exhibit higher performance than Pt/C. Saida et al. synthesized TiO₂ nanosheet modified PtRu/C electrocatalyst and found an increase in electrochemical surface area of PtRu and MOR activity.⁶¹ They recommended by the accelerated degradation tests that the high durability of the catalyst results from the ability of TiO₂ nanosheet to suppress the Ru loss from the catalyst.

3.1.6. Photo-electro-catalysis of TiO₂ for PEFCs

TiO₂ is a semiconductor with a large band gap of 3.0-3.2 eV and an effective photo-catalyst for MOR under UV excitation.⁶² Considering its photo-catalysis and co-electro-catalysis, TiO₂ has been attempted as a photo-electro-catalyst for PEFCs so the synergistic effect of electro- and photo-catalysis can be achieved at the same time in a single fuel cell system.

Mandelbaum et al. investigated the photo-electro-oxidation of methanol, 2-propanol and tert-butyl alcohol on TiO₂ film and proposed a mechanism in which the oxidation of the alcohols is mediated by $\text{-OH}\cdot$ radicals formed by the reaction of surface -OH groups with photogenerated holes.⁶³ Drew et al. deposited TiO₂ semiconductor nanoparticles as a photocatalyst and Pt-Ru nanoparticles as an electrocatalyst on opposite sides of the carbon fiber electrode (CFE) to obtain TiO₂/Pt-Ru hybrid catalyst for MOR.⁶⁴ Figure 8

shows their designed air-breathing direct methanol fuel cell (DMFCs) equipped with quartz window for UV excitation and polarization curves using TiO₂/CFE/Pt-Ru anode and CFE/Pt black cathode. By irradiating the semiconductor hybrid electrode, the peak power density of DMFC was increased by 25%. Although both catalysts carry out MOR independently, an additive effect was still observed. Jia et al. fabricated nanoporous gold supported on TiO₂ and investigated its photo-electro-catalysis for MOR in alkaline medium under UV radiation.⁶⁵ The large photocurrent and almost reversible voltammetric responses show an effective elimination of gold surface passivation because of a pronounced synergistic effect between TiO₂ and gold. The introduction of TiO₂ leads to a 30% decrease of apparent activation energy for MOR. As shown in Figure 9, the methanol electro-oxidation on nanoporous gold and photo-electro-oxidation on TiO₂ at the same time occur in a single system. The reactive intermediates photogenerated on TiO₂ under UV illumination could transfer to the surface of nanoporous gold and undergo further electrocatalytic oxidation, while the reaction intermediates on gold could transfer to TiO₂ for the photo-catalysis. It is worthy to note that the presence of gold could promote the separation of the photoinduced charge carriers in TiO₂, while the presence of TiO₂ could prevent the agglomeration of gold nanoparticles. Wang et al. deposited Pt on TiO₂ nanotube (TNTs) on a Ti substrate by a modulated pulse current technique.⁶⁶ The resultant Pt/TNTs/Ti electrode exhibits an even better performance for methanol oxidation under illumination than the best bi-metallic PtRu catalysts, which can be attributed to the abundance of oxygen-containing species produced by H₂O oxidation on TiO₂ nanotubes under illumination, which removes effectively the intermediate poison CO_{ad} during methanol oxidation.

The presence of TiO₂ can at the same time achieve the synergistic effect of electro- and photo-catalysis in a single fuel cell system, which not only increases catalytic activity and durability of catalysts but also enhances energy utilization efficiency. Undoubtedly, photo-electro-catalysis of TiO₂ is a promising direction to the development of high-performance PEFCs.

3.2. Tungsten oxides (WO_x)

Tungsten oxides (WO_x) are stable in acidic solution and are prepared from ammonium or sodium tungstate and tungsten metal. Tungsten oxide can react rapidly with the active hydrogen adsorbed on Pt to form “hydrogen tungsten bronzes” (Eqs. 5 and 6).⁶⁷ Hydrogen tungsten bronzes have a general formula of H_xWO₃ (0.3 < x < 0.5) and are structurally analogous to sodium tungsten bronzes (Na_xWO₃). They are acid resistant metallic conductors (“pseudo-metals”), which makes them possible to be used in strongly acidic fuel cell environment.



The literature on tungsten oxides in fuel cells can go back to 1960's when Hobbs and Tseung proposed that tungsten oxides could play a co-catalytic role in the anodic oxidation of hydrogen on Pt/WO₃ electrodes by the formation of H_xWO₃.⁶⁸ Later, Tseung group carried out a series of work about WO₃ modified Pt and PtRu catalysts in the electrooxidation of H₂,⁶⁹ CO,⁷⁰ methanol,⁷¹ and formic acid.⁷² They found that the WO₃ modified Pt and PtRu electrodes are much more active and more resistant to poisoning than Pt and PtRu alloy catalysts. The promotional effect of WO₃ was attributed to several

aspects: 1) Uniform dispersion of noble metal nanoparticles on WO_3 . This depends on different preparation methods to some extent. 2) “Hydrogen spillover effect”. It means the formation of hydrogen tungsten bronze and the subsequent oxidation of hydrogen on hydrogen tungsten bronze, which ensures that the Pt active sites can function more efficiently as a dehydrogenation catalyst and that poisons are more readily desorbed from the catalyst surface. 3) A strong resistance to poisoning by intermediates such as CO. The presence of WO_3 could lead to the easy formation of adsorbed water or OH_{ad} and thus oxidize effectively the intermediate poisons.

Since then, various tungsten oxides have been synthesized by various preparation methods and used in various fuel cell applications such as HOR, MOR, EOR, FAOR and ORR.

3.2.1. WO_x

Lalande et al. supported Pt nanocatalysts on WO_x by high energy ball milling technique and found that Pt/WO_x exhibits the comparable CO tolerance to commercial PtRu black in fuel cell tests with H_2 and 100 ppm CO at the anode.⁷³ Lee et al.⁷⁴ and Shafia Hoor et al.⁷⁵ prepared Pt/WO_3 and PtRu/WO_3 nanocatalysts by electrodeposition method; Park et al. fabricated Pt/WO_3 and PtRu/WO_3 nanocatalysts by a multi-sputtering deposition process.^{76,77} They found that the catalytic performance of the Pt/WO_3 and PtRu/WO_3 for MOR is better than Pt and PtRu. The enhanced catalytic activity for MOR relates closely to the presence of alloy nanophases and the spillover effects from tungsten oxides.

Although electrocatalysts supported on WO_3 exhibit some catalytic performance, the low electronic conductivity and surface area of WO_3 lead to much lower catalytic

performance than that for the commercialization of PEFCs. Such problems have been alleviated by the modification of composition and morphology of WO_3 discussed as follows.

3.2.2. Doped WO_3

The doping of WO_3 by other transition metal ions can improve its electronic conductivity and stability in acid medium.⁷⁸ Raghuveer loaded Pt in the $\text{W}_{1-x}\text{Ti}_x\text{O}_3$ ($x = 0, 0.05, 0.09$ and 0.17) and found that the stability of WO_3 in acid medium was found to be improved by the substitution of less Ti^{4+} in the WO_3 framework.⁷⁹ The $\text{Pt-W}_{0.83}\text{Ti}_{0.17}\text{O}_3/\text{C}$ exhibits the best electrocatalytic activity for MOR because of the lower ohmic resistance at the electrode from the accumulation of metallic Ti on the surface. Nagarajan et al. doped WO_3 and TiO_2 to Pt/C and found that the optimized $\text{Pt-WO}_3\text{-TiO}_2/\text{C}$ catalysts show better performance than commercial 10% Pt/C in PEFC,⁸⁰ resulting from the improvement of proton transfer through Pt surface with $\text{WO}_3\text{-TiO}_2$ molecules.

3.2.3. WO_3/C or CNT mixture

In view of the lower specific surface area and conductivity of WO_3 , Zhang et al. prepared the hybrid support WO_3/C and deposited Pd nanocatalysts on the support.⁸¹ As shown in Figure 10, the resultant Pd- WO_3/C catalysts in a large range of WO_3 content between 10 wt% and 65 wt% exhibit much better catalytic activity and stability for FAOR. Especially the one with WO_3 of 20 wt% has twice catalytic activity that of Pd/C catalyst. The presence of WO_3 not only promotes the uniform dispersion of Pd with smaller particle size on the composite support but also regenerates the Pd active sites occupied by

adsorbed/absorbed hydrogen by hydrogen spillover effect and thus markedly accelerates the dehydrogenation of HCOOH on Pd as shown in Eqs. 7-10.



Zhang further explored the ORR behaviors of the Pd-WO₃/C catalyst and found that it shows an ORR activity comparable to the commercial Pt/C catalyst and a higher activity than the Pd/C catalyst prepared with the same method.⁸² The improvement in the catalytic performance is attributed to the small particle sizes and uniform dispersion of Pd on the WO₃/C, the strong interaction between Pd and WO₃, and the formation of hydrogen tungsten bronze which effectively promote the direct 4-electron pathway of the ORR at Pd. Considering the serious effect of methanol crossover on Pt catalysts, the Pd-WO₃/C catalyst because of much higher methanol tolerance and lower price is a promising alternative for ORR to Pt-based catalysts in DMFC. Pereira,⁸³ Maillard⁸⁴ and Roth⁸⁵ reported high CO tolerance of Pt-WO_x/C and Pt-Ru-WO_x/C catalysts for the oxidation of H₂/CO mixtures compared with Pt or PtRu catalysts. Zhang⁸⁶ and Miecznikowski⁸⁷ prepared Pt-WO₃/C and Pt-Sn-WO₃/C catalysts which exhibit excellent catalytic activity and stability for EOR, attributed to the strong interaction between WO₃ and metal nanoparticles, and the large population of reactive oxo groups from WO₃. Rajesh et al. synthesized Pt-WO₃ supported on CNT and found that it exhibits higher activity for MOR than the corresponding Pt/CNT catalyst and commercial Pt and Pt-Ru catalysts,⁸⁸ confirming the existence of the bifunctional mechanism in the presence of WO₃.

Although WO_3/C or CNT composite supports exhibit excellent co-catalytic performance, they still face the same carbon corrosion problem as mentioned in Introduction. One way which takes full advantage of WO_3 and avoids the use of carbon materials is to prepare WO_3 with high specific surface area and conductivity.

3.2.4. Morphological influence of WO_3

The morphology of WO_3 has a markedly influence on its physical properties and electrochemical performance. For example, ordered mesoporous WO_{3-x} has a high conductivity of 1.76 S cm^{-1} comparable to ordered mesoporous carbons (3.0 S cm^{-1}).⁸⁹ The Pt nanocatalysts supported on the ordered mesoporous WO_3 synthesized using mesoporous KIT-6 as a hard template shows high electrocatalytic activity for HOR and much improved resistance to CO poisoning.⁹⁰ The Pt nanocatalysts supported on WO_3 nanoclusters also exhibits excellent electrochemical stability at a high potential (1.6 V for 10 h) compared with that supported on Vulcan XC-72.⁹¹ Recently, Cui et al. synthesized the mesoporous WO_3/C with crystalline framework and high electric conductivity by an in-situ carbonization-replication route using mesoporous silica as a hard template. The composite shows obvious electrocatalytic performance for HOR and demonstrates its potential as a non-noble-metal anode catalyst in PEMFCs.⁹² The Pt nanocatalysts supported on WO_3 microspheres,⁹³ WO_3 nanorods⁹⁴ and nest-like-porous WO_3 hierarchical microspheres⁹⁵ exhibit excellent catalytic performance for MOR because of the strong CO tolerance and special nanostructures of WO_3 . Yan et al. synthesized WO_3 nanobars on carbon by an ionic exchange route and deposited Pt on the WO_3/C support as

ORR electrocatalysts.⁹⁶ The resultant Pt-WO₃/C shows much higher ORR performance than Pt/C.

3.3. Molybdenum oxides (MoO_x)

Molybdenum oxides include five Magneli phases with compositions between MoO₂ and MoO₃.⁹⁷ MoO₂ has a rutile-type structure in which MO₆ octahedra share cores and edges. It has unusual high electronic conductivity because of the short metal-metal bond distance along the direction of edge sharing. Mo₄O₁₁, Mo₈O₂₃ and Mo₉O₂₆ have a basic ReO₃-type structure in which the MO₆ octahedra are joined at cores. They are also electronic conductors. MoO₃ has an orthorhombic structure and is non-conducting. However, it can be electrochemically reduced to a non-stoichiometric and electroconductive H_xMoO₃. Moreover, these oxides are stable in acid solutions. These characteristics of molybdenum oxides make them possible to be used in PEFCs' environment.

Early in 1977, Horkans et al. attempted to use four conducting single crystal molybdenum oxides (MoO₂, Mo₄O₁₁, Mo₈O₂₃ and Mo₉O₂₆) as ORR catalysts in strong acidic media.⁹⁷ Four oxides were found to have some catalytic activity for ORR although they are much lower than the Pt catalyst. Their crystal orientations have a substantial effect on the ORR rate. Since then, molybdenum oxides have attracted a markedly interest in PEFCs' application.

3.3.1. MoO₂

Yan et al. synthesized MoO₂ down to 5 nm on carbon and deposited Pt nanoparticles on the composite support.⁹⁸ The resultant Pt/C-MoO₂ exhibits higher mass activity (187.4 mA mg⁻¹_{Pt}) and stability at 0.90 V vs. RHE for ORR than the commercial Pt/C catalyst (98.4 mA mg⁻¹_{Pt}), attributed to the promotion effect of MoO₂ and the strong interaction between Pt and MoO₂.

3.3.2. MoO₃

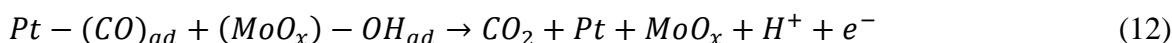
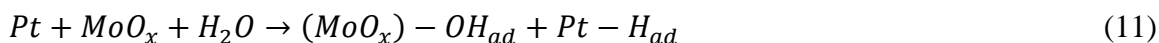
Chen et al. modeled the hydrogen spillover on the MoO₃ (010) in the presence of Pt by density functional theory.⁹⁹ They found that hydrogen can move almost freely on the surface and diffuse into the bulk lattice at ambient temperature, leading to the formation of hydrogen molybdenum bronze. Its high proton mobility results from the immense H-bonding network in the MoO₃ lattice. The formation of hydrogen molybdenum bronze endows MoO₃ with high electronic and proton conductivity, which leads to the possible application of MoO₃ in PEFCs. Justin incorporated MoO₃ into Vulcan XC-72R carbon by solid-state reaction under intermittent microwave heating and deposited Pt nanoparticles on the composite support by microwave assisted polyol process.¹⁰⁰ The Pt-MoO₃/C catalyst exhibits about 128% higher peak current and better stability for MOR than Pt-Ru/C catalyst. The significant agreeable improvement in electrocatalytic activity and stability for MOR is attributed to the strong metal-support interaction between Pt and MoO₃, and the formation of hydrogen molybdenum bronze during the CV measurements, which reduces the CO poisoning of Pt catalysts. Guillén-Villafuerte prepared a core-shell molybdenum substrate with a reduced-Mo core (Mo₂C, MoO₂ and/or Mo⁰) and a MoO₃

shell by a carbothermal reduction method, and employed it as the support of Pt for the oxidation of CO and methanol.¹⁰¹ The resultant Pt/X@MoO₃/C (X = Mo₂C, MoO₂, Mn⁰) especially Pt/Mo₂C@MoO₃/C exhibits the enhanced CO and methanol oxidation by facile OH formation and the electronic effect from the Mo-based supports.

The presence of MoO₃ can significantly enhance the electrocatalytic activity and stability of metal catalysts by the strong metal-support interaction between metal and MoO₃, and the formation of hydrogen molybdenum bronze. However, general preparation methods are difficult to obtain MoO₃ with high specific surface area, which restrains its extensive application in PEFCs. Therefore, developing an effective method to obtain MoO₃ with high specific surface area is a future task.

3.3.3. MoO_x

Usually, molybdenum oxides do not exist in a single phase but in mixed-valence oxides (MoO_x). As Wang reported, there are the Mo⁶⁺ and lower valence state Mo⁵⁺ and Mo⁴⁺ species at the Pt/MoO_x prepared by an electrochemical co-deposition method.¹⁰² The promotion mechanism of MoO_x for MOR was proposed to provide OH species at lower potential for the removal of adsorbed CO poisons as shown in Eqs. 11 and 12.



Elezović et al. prepared MoO_x-Pt/C nanocatalysts by the polyol method combined by the post-deposition of MoO_x and investigated their catalytic performance for MOR and ORR.¹⁰³ The negative shift of MOR peak potential at the MoO_x-Pt/C results from the spillover of oxygen from MoO_x to Pt atoms. The marked improvement in ORR at the

MoO_x-Pt/C is attributed to the synergistic effects because of the formation of an interface between Pt and MoO_x, and by spillover because of diffusion of the reaction intermediates. Muhamad et al. and Tsiouvaras et al. prepared Pt-MoO_x/C and PtRu-MoO_x/carbon nanofibers, respectively, and found that the incorporation of Mo markedly increases CO tolerance of the catalysts.^{104, 105} Liu explored PtMo alloy and MoO_x@Pt core-shell nanoparticles as highly CO-tolerant electrocatalysts for PEFCs.¹⁰⁶ As shown in Figure 11a, distinct underpotential hydrogen adsorption/desorption peaks appear at the MoO_x@Pt core-shell nanocatalysts, while they are absent at the Pt_{0.8}Mo_{0.2} alloy catalyst. It was found from Figure 11b that the MoO_x@Pt core-shell nanocatalysts show much lower onset H₂ oxidation potential (-0.14 V vs. SCE) than the Pt_{0.8}Mo_{0.2} alloy, and the commercial Pt and PtRu catalysts. Moreover, it reaches the diffusion-limited current at 0.1 V vs. SCE, far below that of Pt and PtRu. More importantly, the electronic effect of MoO_x cores on Pt shell was considered to weaken the Pt-CO bond and reduce the oxidation overpotential because MoO_x cores are difficult to provide OH species for the Pt shells to remove CO and regenerate Pt surface based on the bifunctional mechanism. Alcaide et al. investigated the catalytic performance of PtRu-MoO_x/C catalysts with various Mo amount for PEFCs with H₂/CO mixture.¹⁰⁷ They found that the catalyst with a little Mo (1 wt%) has the highest CO tolerance. It was proposed based on the bifunctional mechanism that CO species adsorbed on adjacent Pt atoms to Mo can react easily with the OH species of the MoO(OH)₂ to form CO₂ at a potential lower than 0.25 V. At higher potentials, the active oxygen species on the Ru centers rather than MoO_x are responsible for the removal of CO adsorbed at Pt sites.

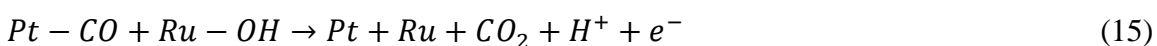
3.3.4. H_xMoO_3

As mentioned in the section about MoO_3 , the promotion effect of MoO_3 is in part because of the formation of hydrogen molybdenum bronze during the CV measurements. Therefore, some researchers directly applied H_xMoO_3 as the promoters of Pt or PtRu for PEFCs. Hou et al. deposited amorphous H_xMoO_3 colloid on Vulcan XC-72 carbon to form a composite support for PtRu nanoparticles as PEFC anode catalysts.¹⁰⁸ The PtRu- H_xMoO_3/C exhibits lower onset potential of CO oxidation and higher HOR current than PtRu/C. It was proposed that hydrogen and CO spillover occur on H_xMoO_3 , which leads to the facile removal of CO by the active water bonded on the H_xMoO_3 based on the bifunctional mechanism. Zhou et al. loaded Pt on CNTs by sodium borohydride reduction in ethylene glycol and modified Pt/CNT with H_xMoO_3 formed by hydrolysis and subsequent reduction of ammonium molybdate.¹⁰⁹ The resultant Pt- H_xMoO_3/CNT exhibits higher catalytic activity for MOR and better CO tolerance than Pt/CNT. To further improve the stability of H_xMoO_3 , Li et al. prepare polyaniline-stabilized Pt- H_xMoO_3 and found that the catalyst exhibits the enhanced catalytic activity and stability for MOR.¹¹⁰

3.4. Ruthenium oxides (RuO_x)

Ruthenium oxides have various forms with various oxidation states and hydrous states. The common Ru(IV) oxides are RuO_2 and RuO_xH_y (or $RuO_2 \cdot xH_2O$). Ruthenium oxides are electrochemically stable within the hydrogen and oxygen evolution region compared with Ru metal which is irreversibly oxidized at potentials higher than 0.8 V vs. RHE. According to the bifunctional mechanism for PtRu catalysts,⁹ Pt dehydrogenates the

chemisorbed methyl moiety in sequential steps to yield a residual Pt–CO fragment that cannot be oxidized to CO₂ at DMFC potentials (Eq. 13); the role of Ru is to dissociate water to create an oxygenation species (Ru–OH) that converts –C≡O fragments on neighboring Pt atoms to CO₂ at lower potentials (Eqs. 14 and 15). Ruthenium oxides can also produce Ru–OH and thus has been proved an effective co-catalyst of Pt for MOR. However, it is still debatable which form of ruthenium (Ru metal, anhydrous RuO₂ or hydrous RuO_xH_y) is the most active co-catalyst of Pt for MOR.



3.4.1. Ruthenium dioxide (RuO₂)

Suffredini et al. prepared Pt-RuO₂ coatings on carbon black substrate by a sol-gel method and they have higher activity for MOR than the commercial PtRu catalyst.¹¹¹ Lasch et al. synthesized RuO₂ with high electronic conductivity and surface area (125 m² g⁻¹) and deposited PtRu nanoparticles on it.¹¹² Interestingly, the PtRu catalyst deposited on the freshly precipitated hydrous RuO₂ exhibits no significant electrochemical activity for MOR, while that on calcined RuO₂ has an activity comparable to the commercial catalyst supported on Vulcan XC-72. Peng et al. compared the catalytic activity of Pt/CNTs, Pt/Ru/CNTs, Pt/RuO₂/CNTs and RuO₂/Pt/CNTs for MOR.¹¹³ It is found that the presence of Ru, no matter in alloy or in oxide, can improve the CO-resistance ability. The Pt/RuO₂/CNTs catalyst exhibits the best activity, indicating that the RuO₂ layer between Pt nanoparticles and CNT support can take full advantage of its CO-resistance ability.

Another role of RuO₂ promotes the uniform distribution of Pt nanoparticles on CNTs to obtain larger ESA. Pylypenko investigated the ruthenium oxides as non-carbon supports for fuel cell catalysts.¹¹⁴ All ruthenium oxide powders exhibit higher corrosion stability than carbon. Full conversion of RuO₂·nH₂O to the RuO₂ phase by post-reduction in a hydrogen atmosphere leads to improved conductivity and corrosion stability.

3.4.2. Hydrus ruthenium oxide (RuO_xH_y or RuO₂·xH₂O)

Hydrus ruthenium oxide (RuO_xH_y or RuO₂·xH₂O) is an excellent mixed proton and electron conductor.¹¹⁵ As Dmowski showed, RuO₂·xH₂O is a composite of anhydrous rutile-like RuO₂ nanocrystals dispersed by boundaries of structural water associated with Ru–O.¹¹⁶ Metallic conduction is supported by the rutile-like nanocrystals, while proton conduction is eased by the structural water along the grain boundaries. The change in oxidation state of Ru in hydrus ruthenium oxide can produce Ru–OH speciation as shown in Eq. 16, expected to dissociate H₂O efficiently and be a promising co-catalyst of Pt for MOR based on the bi-functional mechanism.



Rolison et al. found that although practical PtRu blacks have the same XRD pattern as in an alloy, substantial amounts of hydrus ruthenium oxide is present in the PtRu blacks and cannot be noticed by XRD because of its amorphous property.¹¹⁷ They proposed that hydrus ruthenium oxide, rather than Ru metal or anhydrous RuO₂, is the preferred Ru speciation in these catalysts. As advised by Rolison, the deliberate control of the Ru speciation in PtRu blacks to form RuO_xH_y rather than Ru metal or anhydrous RuO₂ will help improve the catalytic performance of PtRu catalysts. To further highlight the

important role of RuO_xH_y , Long and Rolison investigated the effects of Ru states (Pt^0Ru^0 , $\text{Pt-RuO}_x\text{H}_y$ and Pt-RuO_2) in PtRu catalysts on their catalytic performance for MOR.¹¹⁸ They found that Pt^0Ru^0 has orders of magnitude less activity for MOR than the mixed-phase $\text{Pt-RuO}_x\text{H}_y$. The catalytic activity of $\text{Pt-RuO}_x\text{H}_y$ for MOR exhibits a dramatic loss after the structural water is thermally removed from the hydrous oxide to form RuO_2 . They also show that bulk, rather than near-surface, quantities of RuO_xH_y must accomplish the highest activity for MOR. Chen et al. prepared Pt catalysts supported on hydrous ruthenium oxide by a two-step process and found the resultant $\text{Pt/RuO}_2\cdot x\text{H}_2\text{O}$ shows higher activity for MOR than E-TEK PtRu black catalyst.¹¹⁹ The enhanced performance is attributed to the presence of the amorphous ruthenium oxide rather than Ru^0 , a high dispersion of uniform Pt nanoparticles on the $\text{RuO}_2\cdot x\text{H}_2\text{O}$ support, and the abundance of boundaries between Pt and $\text{RuO}_2\cdot x\text{H}_2\text{O}$. Scheiba employed amorphous hydrous ruthenium oxides as the support for Pt nanoparticles and found that the $\text{Pt/RuO}_2\cdot x\text{H}_2\text{O}$ shows the improved performance in MEA tests compared with PtRu black.¹²⁰ They proposed that the main role of hydrous RuO_2 is to increase the proton conductivity and catalyst utilization in the MEA and its effect on the promotion of CO and methanol oxidation is limited. Selvaganesh et al. deposited Pt nanoparticles on carbon-supported hydrous RuO_2 .¹²¹ The performance of $\text{Pt-RuO}_2/\text{C}$ catalyst degrades by 8% after 10,000 accelerated stress test (AST) cycles, while Pt/C degrades by 60% after 7,000 AST cycles. The introduction of amorphous RuO_2 mitigates the aggregation of Pt particles, prevents their dissolution, and thus improves the catalytic activity and stability.

3.4.3. RuO_x-based composite oxides

To further enhance the catalytic activity and stability of RuO_x-based catalysts, other oxides such as SiO₂ and MnO₂ have been introduced to forming composite supports with RuO_x. Zhou et al. supported RuO₂-MnO₂ composite oxides on multi-wall CNTs by the oxidation-reduction reaction of RuCl₃ and KMnO₄ and deposited Pt nanoparticles on the composite support.¹²² The Pt/RuO₂-MnO₂/CNTs exhibits high catalytic activity for the oxidation of CO and methanol. The introduction of MnO₂ was found to improve the proton conductivity and ESA of the catalyst. Lo et al. loaded RuO₂ onto ordered mesoporous SiO₂ matrix (SBA-15) to form SiO₂-RuO₂ composite oxide as a support of Pt for PEFCs.¹²³ The ideal SiO₂-RuO₂ (1:1 mol.) support has a BET surface area of 305 m² g⁻¹ and an electronic conductivity of 24 S cm⁻¹. The SiO₂-RuO₂ shows 10 fold higher electrochemical stability than Vulcan XC-72R carbon after an accelerated stability test involving 10,000 potential cycles between 1 and 1.5 V. Zheng et al. prepared Pt/RuO₂-SiO₂/C as the anode catalyst for PEFCs and found that it exhibits better wettability of MEA than Pt/SiO₂/C and Pt/C.¹²⁴ The combination of hydrophilic SiO₂ and co-catalytic RuO₂ increases both the activity and the stability of non-humidification MEA during a long-time run.

3.4.4. Morphological influence of RuO₂

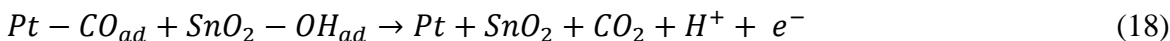
The morphology of RuO₂ has an obvious effect on its catalytic activity. As reported in the literature,¹²⁵ there are two active oxygen species: bridge O atoms and on-top oxygen atoms. The weak oxygen surface bonding of bridging O atoms on RuO₂(110) compared with the strongly chemisorbed oxygen on Ru(0001) for metallic Ru leads to much higher

activity on RuO₂ for CO oxidation than metallic Ru catalysts. Considering that the nanorods principally exhibit the (110) planes of sidewall, Gu et al. deposited Pt nanoparticles on amine-functional RuO₂ nanorods by a simple two-step process to form the Pt/RuO₂ nanorods catalyst.¹²⁶ The presence of RuO₂ nanorods markedly increases the electrochemical activity of Pt/RuO₂ for MOR. Saida et al. prepared RuO₂ nanosheets by chemical exfoliation of a layered potassium ruthenate and deposited it on Pt/C.¹²⁷ The RuO₂ nanosheet modified Pt/C exhibits an excellent catalytic and stability, which is because of that RuO₂ nanosheets can improve the CO-resistant ability of the catalyst. Ruthenium oxides have exhibited excellent catalytic activity for alcohol oxidation based a bifunctional mechanism. Although the high price restrains their extensive use in PEFCs, the study on them has a significant guide for the insight into the mechanism of alcohol oxidation because of their various forms with various oxidation states and hydrous states.

3.5. Tin oxides (SnO_x)

PtSn- and PdSn-based electrocatalysts have shown excellent catalytic performance for EOR and FAOR in PEFCs.^{128, 129} Sn can function as a co-catalyst based on bifunctional and/or electronic mechanisms. For example, the presence of Sn leads to the lowering of Pd(3d) binding energy and the negative shift of d-band center, and thus produces an electronic effect, which weakens the bond strength of intermediates adsorbed on the catalysts and promotes the Pd catalysts for FAOR.¹²⁸ However, SnO₂ often exists on the surface of Sn-based catalysts, which probably results from the oxidation of Sn nanoparticle surface and/or from general preparation procedures. Therefore, the catalytic function of SnO₂ has attracted researchers' interests. SnO₂ is an n-type semiconductor

with higher electronic conductivity. It has good corrosion resistance in acid media and thus is expected to be stable in the work conditions of PEFCs. It has also abundant hydroxyls on the surface, which is possible in depressing the CO poisoning based on the bifunctional mechanism as shown in Eqs. 17 and 18.¹²⁹



3.5.1. SnO₂

Waki et al.¹³⁰ and Matsui et al.¹³¹ prepared Pt-SnO₂ nanocatalysts and found that they exhibit lower onset potential for CO oxidation than Pt/C. The high CO tolerance results from the promotion effect of the Sn(II)/Sn(IV) redox couple and highly homogeneous dispersion of Pt on SnO_x. Sandoval-González et al. also found that the Pt-SnO₂/C prepared by microwave assisted polyol method shows better catalytic activity and stability for MOR than commercial PtRu/C catalyst, which results from the bifunctional property of Pt and SnO₂.¹³² Jiang et al. employed the size-controllable SnO₂ nanoparticles prepared by heating ethylene glycol solutions containing SnCl₂ to prepare carbon-supported Pt-SnO₂ catalyst.¹³³ The catalyst exhibits surprisingly high performance for EOR (maximum power density: 80 mW cm⁻²) compared with that of Pt/C (maximum power density: 10 mW cm⁻²), and this improvement is attributed to the presence of both adequately large Pt ensembles for ethanol dehydrogenation and C–C bond splitting and of tin oxide for OH generation.¹³⁴ Silva et al. prepared Pt-SnO₂/C with various Pt:Sn atomic ratios (75:25, 50:50 and 25:75) using electron beam irradiation.¹³⁵ The Pt-SnO₂/C with Pt:Sn atomic ratios of 50:50 shows the best performance for EOR in acid media. Ternary

Pt-Rh-SnO₂/C catalyst has further been synthesized by depositing Pt and Rh atoms on carbon-supported SnO₂ nanoparticles for EOR in acid media.^{136, 137} As shown in Figure 12a, Pt-Rh-SnO₂/C exhibits a considerably higher activity than Pt-SnO₂/C, highlighting the importance of Rh component. Figure 12b shows that the current density of Pt-Rh-SnO₂/C at 0.3 V is more than two orders of magnitude larger than that of the commercial Pt/C. Moreover, it also exhibits a high current density of 7.5 mA cm⁻² at 0.3 V while PtRu/C has a negligible current density at the same potential (Figure 12c). The chronoamperometric result in Figure 12d confirms that the much higher stability of Pt-Rh-SnO₂/C than Pt/C. Unusually high catalytic performance of the composite catalyst is attributed to the interaction among three constituents: Pt for adsorption of ethanol molecules, Rh for ease of C–C bond splitting, and SnO₂ for the oxidative removal of CO_{ad} produced because of C–C bond splitting.

3.5.2. Doped SnO₂

Although SnO₂ shows good co-catalytic activity, enhancing its conductivity and stability by doping could further improve its catalytic performance. Lee et al. prepared Pt nanocatalysts supported on Sb-doped SnO₂.¹³⁸ The Pt/Sb-SnO₂ catalyst exhibits higher catalytic activity for MOR and EOR than Pt/C, which is attributed to better dispersion of Pt particles on the Sb-SnO₂ support and the bifunctional effect of SnO₂. Much better stability of Pt/Sb-SnO₂ results from higher corrosion resistance of Sb-SnO₂ and the strong interaction between Pt and Sb-SnO₂. Oliveira Neto et al. deposited Pt nanoparticles onto the commercial Sb-doped SnO₂ and carbon black by a polyol process.¹³⁹ The resultant Pt/Sb-SnO₂-C is more active for EOR than Pt/C, Pt/Sb-SnO₂ and Pt/Sb-SnO₂-C. The

presence of carbon black and Sb doping seems to collaboratively increase the electron conductivity and surface area of SnO₂. Takasaki et al. doped SnO₂ with hypervalent Nb⁵⁺ and hypovalent Al³⁺ ions and employed the doped SnO₂ to obtain Pt/Nb-SnO₂ and Pt/Al-SnO₂ catalysts for ORR.¹⁴⁰ They found that Pt/Sn_{0.95}Nb_{0.05}O₂ exhibits higher kinetic current than Pt/SnO₂, while Pt/Sn_{0.95}Al_{0.05}O₂ is inactive for ORR. Although the catalytic activity of Pt/doped SnO₂ catalysts is still lower than that of Pt/C, they show better durability due to their high anticorrosion ability.

3.5.3. Morphological influence of SnO₂

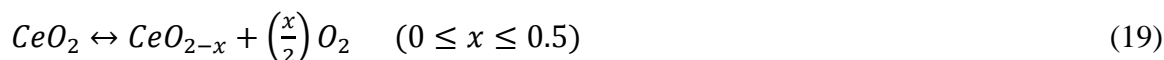
Morphologies of SnO₂ have a marked effect on their physical properties and catalytic performance. For example, the nanofiber morphology can provide an easy access to electron transfer along an alignment compared with nanoparticles and thus have higher electron conductivity. The mesoporous morphology is favorable for the mass transfer of fuel molecules in PEFCs. Saha et al. directly grew SnO₂ nanowires on carbon paper by a thermal evaporation method and deposited Pt and PtRu nanoparticles on the nanowires by potentiostatic electrodeposition method.^{141, 142} The resultant Pt/SnO₂ nanowires/carbon paper and PtRu/SnO₂ nanowires/carbon paper show higher mass and specific activity for MOR and better CO tolerance than Pt and PtRu deposited on glassy carbon, respectively, attributed to the unique 3D structure and bifunctional and/or electronic properties of SnO₂ nanowires. Suryamas et al. in-situ grew Pt nanoparticles on the electrospun SnO₂ nanofibers.¹⁴³ The as-prepared Pt/SnO₂ nanofibers exhibit obvious HOR activity while inhibiting ORR. Dou et al. synthesized SnO₂ nanoclusters with parallel nanorods using a hard template and deposited Pt nanoparticles on it to form Pt/SnO₂.¹⁴⁴ The Pt/SnO₂

nanoclusters exhibit comparable catalytic activity to Pt/C and superior electrochemical stability for PEFCs, which results from the high surface area and co-catalytic effect of SnO₂ nanoclusters. Zhang et al. synthesized mesoporous SnO₂ with a large surface area of 205 m² g⁻¹ as Pt nanoparticles.¹⁴⁵ The electrochemical stability of Pt/SnO₂ because of the strong interaction between Pt and SnO₂ is significantly improved compared with the commercial Pt/C while showing comparable catalytic activity to that of Pt/C.

SnO₂ has demonstrated its significant role in alcohol oxidation based on a bifunctional mechanism and/or an electronic effect. However, further enhancing its stability in strong acid media and increasing its specific surface area may bring its full potential.

3.6. Cerium oxide (CeO₂)

CeO₂, as a rare earth oxide with a fluorite cubic structure, has widespread applications such as automotive catalysts, electrodes for sensors, oxygen conductors in solid oxide fuel cells, ultraviolet blocking components in cosmetics and abrasives in chemical-mechanical planarization.¹⁴⁶⁻¹⁴⁸ CeO₂ has two interesting features. First, it can switch between Ce⁴⁺ and Ce³⁺ oxidation states depending on whether it is present in an oxidizing or reducing atmosphere (Eq. 19). Second, it contains many oxygen vacancies within its structure leading to high oxygen mobility. The ability of CeO₂ to store, transport and release oxygen makes it possible for ORR and the oxidation of adsorbed intermediate CO during alcohol oxidation. According to the thermodynamic data in Pourbaix's "Atlas of Electrochemical Equilibria", CeO₂ has lower stability in strong acid media. The strong interaction between CeO₂ and metal such as Pt, and/or the doping of CeO₂ by other metal ions is expected to mitigate this problem.



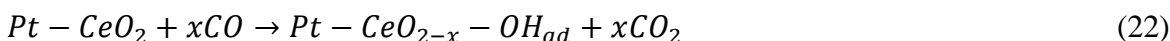
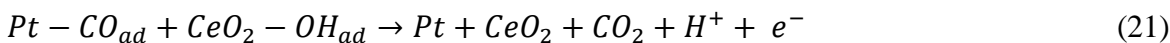
3.6.1. CeO₂

Early in 1998, a Japanese patent reported that adding either zirconium oxide/cerium oxide or vanadium oxide into PEFCs electrodes largely increased air utilization at a cell voltage of 0.6 V.¹⁴⁹ Since then, CeO₂ as an oxygen storage material has been explored in various PEFC applications.

Yu et al. incorporated nanophase CeO₂ to Pt/C for ORR and found that the introduction of 1 wt% CeO₂ increases the local oxygen concentration in the air atmosphere and eases the mass transport of reactant oxygen molecules to Pt, leading to an agreeable improvement in the performance of a DMFC.¹⁵⁰ Xu et al. modified Pt/C with CeO₂ by sol-gel and dipping method, and found that the modification of CeO₂ enhances the ORR activity for PEFCs.¹⁵¹ They proposed a catalytic mechanism of CeO₂ where CeO₂ is first reduced in cathode by an electrochemical reaction, then is oxidized by an ORR intermediate H₂O₂ to its original state, and this cyclic process of CeO₂ promotes the reduced rate of oxygen and thus the PEFC performance. Lee et al. further dispersed PtCo alloy and CeO_x on carbon support by a modified colloid method and found that the PtCo-CeO_x/C exhibits better catalytic performance for ORR than PtCo/C and Pt/C.¹⁵² Based on the XPS analysis, the CeO_x consists of a CeO₂ core and a Ce₂O₃ shell. The unsaturated Ce₂O₃ phase of the CeO_x surface was proposed to ease the adsorption/desorption of oxygen, leading to an enhanced oxygen supply to the PtCo alloy. Xu et al. studied the Pt-CeO₂/C catalyst for the electrooxidation of alcohols (methanol, ethanol, glycerol, ethylene glycol) in alkaline solution.^{153, 154} The addition of CeO₂ to Pt/C catalysts was

found to significantly improve the catalytic performance and CO resistance ability. CeO₂ was proposed to facilitate the formation of OH_{ad} species at lower potential for facile removal of CO_{ad} poison. They further investigated the Pt/C and Pd/C catalysts modified with CeO₂ for EOR in alkaline media.¹⁵⁵ All Pt/C and Pd/C catalyst modified with CeO₂ show higher activity than the commercial E-TEK Pt/C. The catalysts with a weight ratio of noble metal (Pt, Pd) to CeO₂ of 2:1 have the highest catalytic activity for EOR. Neto et al. prepared PtSn-CeO₂/C by an ethylene glycol reduction method and found that the catalyst with 15 wt% of CeO₂ exhibits significantly higher performance for EOR than PtSn/C catalyst.¹⁵⁶ They further found by FTIR that the principle products at PtSn/C are acetaldehyde and acetic acid, while they at PtSn-CeO₂/C are CO₂ and acetic acid, which means that the addition of CeO₂ leads to a more complete oxidation of ethanol molecules.¹⁵⁷ Yu et al. prepared Pt-CeO₂/C composite catalyst by ultrasonically mixing Pt/C (or Pt/CNT or PtRu/C) and CeO₂.¹⁵⁸ CeO₂ improves almost all Pt based catalysts for the electrooxidation of almost all small organic molecular (methanol, ethanol, ethylene glycol and glycerol). The reaction resistance between Pt and alcohols is decreased markedly in the presence of CeO₂. CeO₂ with a particle size of 21 nm was found to exhibit the best promotion effect. Takahashi et al. prepared Pt-CeO₂/C by a co-impregnation method and found that it as the anode of DMFCs exhibits better performance such as lower onset potential and activation energy, and higher peak current density than Pt-Ru/C alloy catalyst, which can avoid using rare metal Ru.¹⁵⁹ Scibioh et al. investigated the promotion effect of CeO₂ for Pt/C for MOR and found that an optimum composition of 40 wt% Pt - 9 wt% CeO₂/C exhibits higher activity than 40 wt% Pt/C.¹⁶⁰ The promotion effect of CeO₂ was proposed to ease the removal of strongly adsorbed

intermediate CO based on bifunctional mechanism (Eqs. 20 and 21) and intrinsic mechanism (Eq. 22).



To further understand the promotion effect of CeO₂, Ou et al. examined the microstructure and metal-oxide interaction of Pt-CeO₂/C with various atomic ratio of Pt/Ce by high-resolution TEM and electron energy loss spectroscopy (EELS).¹⁶¹ As shown in Figure 13a, the value of I_{M4}/I_{M5} (I_{M4}/I_{M5} = 1.25 for Ce⁴⁺; I_{M4}/I_{M5} = 0.95 for Ce³⁺) decreases from 1.21 to 1.10 with Pt content, which means that the CeO₂ support are partly reduced by Pt. Meanwhile, the Pt O_{2,3} edge shifts to lower energy loss, while the Pt N_{6,7} edge slightly shifts in the opposite direction with Pt content (Figure 13b), which means the appearance of Pt cations accompanied by the reduction of CeO₂ support. The EELS study shows the existence of strong Pt-CeO₂ interaction by the redox reaction between Pt and CeO₂ and the increase of the Pt-CeO₂ interaction with the atomic ratio of Pt/Ce. The strong metal-support interaction can contribute to the promotion effect of CeO₂ for MOR.

3.6.2. Doped CeO₂

It is accepted usually that the addition of ZrO₂ to CeO₂ can improve the oxygen storage capacity, redox property and thermal resistance of CeO₂, while the presence of some rare-earth oxides such as Sm₂O₃ in the lattice of CeO₂ can increase the oxygen buffering action from the air feed. The introduction of doped CeO₂ is expected to affect the catalysts' performance. Xu et al. prepared Ce_{0.8}Zr_{0.2}O₂ and V₂O₅, and mixed them with E-

TEK Pt/C as the cathode catalysts for PEFCs.¹⁶² As a result, 14.9 wt% of $\text{Ce}_{0.8}\text{Zr}_{0.2}\text{O}_2$ in Pt/C enhanced the performance of fuel cells, while the incorporation of V_2O_5 largely decreased the performance. Bai et al. also prepared Pt- CeO_2/C and Pt- $\text{Ce}_x\text{Zr}_{1-x}\text{O}_2/\text{C}$ with various Ce/Zr ratio and found that the introduction of CeO_2 and $\text{Ce}_x\text{Zr}_{1-x}\text{O}_2$ leads to the enhanced mass activity and specific activity for EOR compared with Pt/C, which results from their CO-resistance ability based on bifunctional mechanism.¹⁶³ The catalyst with cubic structure $\text{Ce}_x\text{Zr}_{1-x}\text{O}_2$ has higher catalytic activity than that with tetragonal structure $\text{Ce}_x\text{Zr}_{1-x}\text{O}_2$. Choi et al. prepared $\text{Ce}_{0.8}\text{Sm}_{0.2}\text{O}_2$ -modified Pt/C catalyst and compared its catalytic performance as cathode catalysts of DMFCs with CeO_2 -modified Pt/C and blank Pt/C.¹⁶⁴ The presence of a trace of Sm_2O_3 in CeO_2 -modified Pt/C has dramatically improved the performance of DMFCs with air as the oxidant at the cathode, attributed to the high methanol tolerant behavior and the availability of higher local concentration of oxygen accelerated by Sm_2O_3 and CeO_2 from air.

The ability of CeO_2 to store, transport and release oxygen forecasts its potential in ORR and alcohol oxidation. However, its lower stability in strong acid media restrains its extensive use in PEFCs, and is expected to be mitigated by increasing the interaction between CeO_2 and metal nanocatalysts, and by doping with other metal ions.

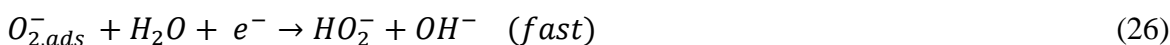
3.7. Manganese oxides (MnO_x)

It is well known that manganese oxides (MnO_x) have many forms: MnO , Mn_3O_4 , Mn_2O_3 , MnOOH , Mn_5O_8 and MnO_2 . Mn changes oxidation states from +2, +3 to +4 near the equilibrium potential for the ORR. In addition, manganese is an inexpensive, earth-abundant element, and thus is scalable for large-scale energy applications. Early in the

1970's the electrochemical reduction of O_2 was found to occur through reduction and oxidation of the redox couple Mn^{4+}/Mn^{3+} .¹⁶⁵ Since then, many researchers have studied the ORR activity of manganese oxides in low temperature alkaline fuel cells.

3.7.1. MnO_2

Lima et al. investigated the ORR activity of MnO , Mn_3O_4 and MnO_2 dispersed on Vulcan XC72 carbon in alkaline medium.^{166, 167} The electrocatalytic activity is related to the mediation processes involving the reduction of Mn(IV) to Mn(III) (Eq. 23), followed by the electron transfer of Mn(III) to oxygen (Eq. 24) and by a disproportionation reaction of the HO_2^- species in the MnO_x (Eq. 26). The overall reaction is a 2-electron ORR reaction. In-situ XANES results show that the Mn(IV) species is MnO_2 and the Mn(III) is most like $MnOOH$.



Zhao et al. prepared MnO_2 modified MWCNTs and supported Pd nanoparticles on the MnO_2 /MWCNTs.¹⁶⁸ The resultant Pd- MnO_2 /MWCNTs catalyst exhibits higher electrocatalytic activity and stability for MOR in alkaline media than Pd/MWCNTs and Pd/Vulcan XC-72 carbon black. MnO_2 is a polymorphic material with a variety of structures such as α , β and γ forms. Cheng et al. found that the catalytic performance of MnO_2 for ORR catalysts in alkaline media depends both on the crystallographic structures (α - > β - > γ - MnO_2) and morphology (nanospheres/nanowires >

microparticles).¹⁶⁹ The Ni nanoparticles deposited on α -MnO₂ nanowires shows an excellent activity and a quasi-4-electron transfer process for ORR. They further prepared oxygen-vacant MnO₂ by merely heating MnO₂ in Ar or air and found the presence of oxygen vacancies enables more positive potential, larger current and lower peroxide yield.¹⁷⁰

3.7.2. MnOOH

Ohsaka group have carried out many studies on the catalytic mechanism of MnOOH for ORR in alkaline media. They compared the catalytic performance of Mn₂O₃, Mn₃O₄, Mn₅O₈ and MnOOH for ORR in alkaline solution and found that MnOOH has highest catalytic activity, related to the disproportionation of HO₂⁻.¹⁷¹ They further found that MnOOH is involved in sequent disproportionation of the electrochemical reduction intermediates such as O₂⁻ and HO₂⁻.¹⁷² MnOOH has excellent catalytic activity not only for the disproportionation of the produced O₂⁻ into O₂ and HO₂⁻, but also for that of the produced HO₂⁻ into O₂ and OH⁻. They further electrodeposited MnOOH on Pt electrodes and found that the introduction of MnOOH leads to the significant positive shift of the ORR onset potential compared to the bare Pt electrode.¹⁷³ As shown in Figure 14A, no obvious change of the binding energies of Pt4f means that the electronic structure of Pt surface remains unchanged after loading of MnO_x. The positive shift of the binding energy of Mn2p in Figure 14B shows that Mn exists in a cationic state rather than in an elemental state. The change of O1s in Figure 14C is attributed to the presence of the oxygen in hydroxide and oxide forms in MnOOH. According the rotating ring-disk electrode results, they proposed that the adsorption orientation of oxygen molecules

changes from parallel orientation at the bare Pt electrode to the mixed orientation of the parallel and end-on modes at the nano-MnO_x/Pt electrode (Figure 14D), leading to more adsorption of O₂ molecules on MnO_x/Pt and thus an increase in the pre-exponential factor of the Arrhenius equation for the ORR. Therefore, higher reaction rate is observed as a positive shift of the onset potential of the ORR.

3.7.3. Mn₂O₃

Gorlin et al. prepared a nanostructured Mn(III) oxide thin film on a glassy carbon by a potentiostatic electrodeposition method.¹⁷⁴ As shown in Figure 15, this non-noble catalyst exhibits an excellent bifunctional catalytic activity for ORR and oxygen evolution reaction (OER) in alkaline solution. Its catalytic performance is comparable to those of noble metal nanoparticle catalyst such as Pt, Ru and Ir.

3.7.4. Mn₃O₄

Kim et al. employed the galvanic replacement between Mn₃O₄ surface and PtCl₄²⁻ to immobilize a high density of ultrathin Pt nanocrystals uniformly on Mn₃O₄ nanoparticles.¹⁷⁵ The resultant Pt/Mn₃O₄ nanocomposite shows highly enhanced specific activity and durability for ORR in acidic solution compared with those of the commercial Pt/C catalyst. Gorlin et al. explored Mn₃O₄ on porous glassy carbon (pGC) as a non-noble metal catalyst for ORR in alkaline media.¹⁷⁶ As shown in Figure 16a, the MnO/GC and MnO/pGC exhibit little improvement in ORR activity compared with their corresponding bare carbon, while the Mn₃O₄/pGC shows significant improvement both in the onset potential (0.8 V) and the limiting current. Moreover, the ORR proceeds through 4-

electron pathway on $\text{Mn}_3\text{O}_4/\text{pGC}$ as on Pt/C (Figure 16b). The Tafel slopes of the MnO/pGC and $\text{Mn}_3\text{O}_4/\text{pGC}$ catalysts are similar to that of Pt/C in the range of 80-90 mV decade⁻¹ (Figure 16c). The $\text{Mn}_3\text{O}_4/\text{pGC}$ exhibits a specific activity of 3700 $\mu\text{A cm}^{-2}_{\text{cat}}$ and a mass activity of 3100 $\text{A g}^{-1}_{\text{cat}}$ at 0.75 V (Figure 16d).

3.7.5. MnO

Tan et al. prepared MnO-containing mesoporous nitrogen-doped carbon (m-N-C) nanocomposite by manganese oxides as an in-situ template for carbon coating and explored its catalytic activity for ORR in alkaline solution.¹⁷⁷ As show in Figure 17a and b, the MnO-m-N-C composite catalyst exhibits higher onset potential, half-wave potential and limitation current plateau than the blank m-N-C, MnO and the physical mixture of m-N-C and MnO catalysts, indicative of the synergistic effect between MnO and m-N-C. The calculated electron transfer number of 3.84 from the slopes of Koutecky-Levich plots (Figure 17c and d) suggests a dominant 4-electron pathway on the MnO-m-N-C composite catalyst. It also exhibits superior stability and methanol tolerance to a commercial Pt/C catalyst.

3.7.6. Morphological influence of MnO_x

Yang et al. prepared nanoporous amorphous manganese oxide by an aqueous redox sol-gel method and studied its catalytic performance for ORR in alkaline media.¹⁷⁸ A current density of more than 100 mA cm^{-2} is reached with a low catalyst loading of 0.85 mg cm^{-2} , attributable to high concentration of lattice defects and active sites, increased composition freedom and higher corrosion resistance. Nanoporous morphology favors the design of

effective gas diffusion electrodes. Rebello et al. prepared MnO_x octahedral molecular sieves supported carbon and mixed it with Ru/C.¹⁷⁹ The resultant Ru/ MnO_x /C was found active for MOR, associated with the presence of the $\text{Mn}^{4+}/\text{Mn}^{3+}$ redox couple and lattice oxygen. Ohno et al. prepared H_3O^+ -form regularly stacked and randomly restacked MnO_x nanosheets for ORR in alkaline media.¹⁸⁰ The catalysts exhibit a high onset potential of 0.97 V and a high 4-electron reduction efficiency of 99%, which is higher than Mn_2O_3 and MnO_2 , and comparable to 20% Pt/C catalyst. The high ORR activity results from an increase in the numbers of the ORR active sites and much H_2O in the interlayers and on the surface of the nanosheets. El-Deab et al. prepared Pt modified with MnO_x nanorods and found that the Pt/ MnO_x results in a significant improvement in the electrocatalytic activity for FAOR.¹⁸¹ The presence of MnO_x eases the charge transfer during the direct oxidation of formic acid to CO_2 and suppresses the formation of poisoning intermediate CO in indirect pathway. Sun et al. coated β - MnO_2 nanorods with Pd nanoparticles for ORR in alkaline media.¹⁸² The resultant Pd@ MnO_2 catalyst exhibits a close onset potential and limiting current density to the Pd black. However, its mass activity is 2.5 times higher than that of the Pd black.

Although manganese oxides have been applied extensively for PEFCs and showed obvious catalytic activity for ORR, it is still debatable which form of manganese oxides has the best catalytic activity for ORR because of their complex valency. In-depth exploration on their ORR mechanism and extensive search for effective ORR compositions are crucial.

3.8. Perovskite oxide (ABO₃)

3.8.1. Structure and property

Perovskite-type oxides, originating from a mineral having a composition of CaTiO₃, have a general formula ABO₃ and a cubic structure with space group Pm3m-O_h in an ideal case.¹⁸³ As shown in Figure 18, A is the cation with a larger ionic radius and has twelve coordination to oxygen atoms; B is the cation with a smaller ionic radius and has six coordination to oxygen atoms. A and O form a cubic closest packing, while B is contained in the octahedral voids of oxygen atoms, in which the partial substitution of cations in A and B sites can lead to a variety of compounds with a formula of A_{1-x}A'_xB_{1-x}B'_xO₃. The flexible structure, high thermal stability, low cost, facile preparation and especially variable valency, stoichiometry and vacancy make perovskite-type oxides promising in wide applications such as heterogeneous catalysis, chemical sensors, magnetic devices, and energy storage and conversion.¹⁸⁴⁻¹⁸⁶

3.8.2. Application in alkaline PEFCs

As far back as 1984, Bockris and Otagawa found that the catalytic activity of oxygen evolution reaction on perovskites relates to the number of transition metal *d*-electrons and the occupancy of the antibonding orbitals of M^Z-OH, and predicted a volcano relationship for oxygen evolution on perovskites.¹⁸⁷ Since then, many researchers have studied the ORR activity of perovskite-type oxides in low temperature alkaline fuel cells.

Hammouche et al. prepared La_{1-x}Ca_xCoO₃ (0 ≤ x ≤ 0.6) by a sol-gel process and found that the ORR reaction rate and electrode active surface area arrive at a maximum when x

= 0.4.¹⁸⁸ Tolloch et al. investigated the catalytic behaviors of $\text{La}_{1-x}\text{Sr}_x\text{MnO}_3$ (where $x = 0, 0.2, 0.4, 0.6, 0.8$ and 1.0) for ORR in 1 M KOH and found that $\text{La}_{0.4}\text{Sr}_{0.6}\text{MnO}_3$ exhibits the highest catalytic activity which approaches that of Pt black.¹⁸⁹ Suntivich et al. employed a thin-film rotating disk electrode to compare the ORR activity of LaNiO_3 , $\text{LaCu}_{0.5}\text{Mn}_{0.5}\text{O}_3$ and $\text{La}_{0.75}\text{Ca}_{0.25}\text{FeO}_3$.¹⁹⁰ As a result, the specific activity of LaNiO_3 is much higher than that of $\text{LaCu}_{0.5}\text{Mn}_{0.5}\text{O}_3$ and $\text{La}_{0.75}\text{Ca}_{0.25}\text{FeO}_3$, and is competitive with the current Pt-based catalysts. Sunarso et al. investigated the ORR performance of LaMO_3 and $\text{LaNi}_{0.5}\text{M}_{0.5}\text{O}_3$ ($M = \text{Ni, Co, Fe, Mn}$ and Cr) catalysts.¹⁹¹ For LaMO_3 , the ORR activity increases in the order of $\text{LaCrO}_3, \text{LaFeO}_3, \text{LaNiO}_3, \text{LaMnO}_3$ and LaCoO_3 ; For $\text{LaNi}_{0.5}\text{M}_{0.5}\text{O}_3$, the ORR activity increases in the order of $\text{LaNi}_{0.5}\text{Fe}_{0.5}\text{O}_3, \text{LaNi}_{0.5}\text{Co}_{0.5}\text{O}_3, \text{LaNi}_{0.5}\text{Cr}_{0.5}\text{O}_3$ and $\text{LaNi}_{0.5}\text{Mn}_{0.5}\text{O}_3$. In all the catalysts, LaCoO_3 shows the largest ORR current density and most positive onset potential. In $\text{LaNi}_{0.5}\text{M}_{0.5}\text{O}_3$, Mn has the best promotional effect on LaNiO_3 . Wang et al. reported a comparative study of the ORR mechanism on LaBO_3 ($B = \text{Mn, Fe, Cr}$) by first-principle calculations based on density functional theory and found that the order of the ORR activity is $\text{LaMnO}_3 > \text{LaCrO}_3 > \text{LaFeO}_3$.¹⁹² Singh et al.¹⁹³ and Poux et al.¹⁹⁴ investigated the electrocatalytic performance of polypyrrole/ $\text{La}_{1-x}\text{Sr}_x\text{MnO}_3$ ($0 \leq x \leq 0.4$) and perovskite (LaCoO_3 and $\text{La}_{0.8}\text{Sr}_{0.2}\text{MnO}_3$)/carbon composite electrodes for ORR, respectively. The presence of polypyrrole and carbon markedly enhance the electrocatalytic activity of perovskites by improving their conductivity.

Although an increased progress has been made in the application of perovskite-type oxides in ORR in alkaline fuel cells, there is still lack of a fundamental understanding of the ORR mechanism in perovskite-type oxides. Because of their structural flexibility,

perovskites have a large number of composition possibilities, which makes it difficult to reach a consensus on the relation between material structure and catalytic performance. Moreover, it is really a great challenge to pick a best perovskite electrocatalyst for ORR in terms of activity, durability, cost and other practical factors governing commercial applications from such a big family.

Shao-Horn, Gasteiger and colleagues identified an “activity descriptor” for predicting electrocatalytic activity of perovskites based on the electronic factors of the B-site metal. They applied the thin-film method to assess the ORR activity of 15 perovskite-type oxides with various A-sites ($\text{La}_{1-x}\text{Ca}_x\text{BO}_3$, $\text{La}_{1+x}\text{BO}_{3+x}$) and B-site ($\text{LaB}_{1-x}\text{B}'_x\text{O}_3$) substitutions.¹⁹⁵ As seen from Figure 19, the perovskite oxides with a moderate e_g -filling ($e_g \approx 1$) such as LaMnO_3 yield higher ORR activity as other oxides with either too little (LaCrO_3 with $e_g = 0$) or too much e_g electron filling (LaFeO_3 with $e_g = 2$). They demonstrated that the ORR activity for oxide catalysts primarily correlates with σ^* -orbital (e_g) occupation and the extent of B-site transition metal-oxygen covalency by influencing the competition between $\text{O}_2^{2-}/\text{OH}^-$ displacement and OH^- regeneration on surface transition metal ions, showing that tuning surface electronic structure features such as transition-metal e_g -filling and covalency is a promising strategy in developing highly active non-noble-metal-containing oxide catalysts for ORR in electrochemical conversion and storage devices.

4. Conclusions and Perspectives

In the present review, we have summarized the development of metal oxide-based electrocatalysts for PEFCs. For Titanium oxides, stoichiometric TiO_2 , sub-stoichiometric

Magneti phase titanium oxides, Nb- and Mo-doped TiO_2 and TiO_2 -carbon composites have been used to display the effect of composition on their catalytic performance; The morphology of TiO_2 such as nanotubes, nanotube arrays and nanosheets have also marked influence on their catalytic performance. Because of its special semiconductor property the synergistic photo- and electro-catalysis of TiO_2 has been demonstrated. For Tungsten oxides and Molybdenum oxides, we have also shown the effects of compositions (doped and undoped WO_x , doped and undoped MoO_x , and WO_x/C and MoO_x/C composites) and morphologies (mesopores and nanorods) on their catalytic performance. We have also emphasized the influence of hydrogen spillover effect by the formation of hydrogen tungsten/molybdenum bronze. For Ruthenium oxides as a model cocatalyst, we have elaborated the effects of various oxidation states and hydrous states based on bi-functional mechanism. For Tin oxides and Cerium oxides, we have discussed the effects of doped and undoped oxides on their catalytic performance. The above-mentioned oxides because of their stability in acidic media are suitable co-catalysts and supports for PEFCs in acid media, while manganese oxides and perovskite oxides can be used as non-noble metal catalysts for PEFCs in alkaline media. For Manganese oxides, we have demonstrated the application of various oxide forms such as MnO_2 , MnOOH , Mn_2O_3 , Mn_3O_4 and MnO as well as various morphologies. For Perovskite oxides, we have shown their general structure and property, and application in alkaline PEFCs. Because of their super structural flexibility, an important paper by Shao-Horn and Gasteiger has been picked out to show how to develop highly active perovskite oxide catalysts by tuning surface electronic structure features such as transition-metal e_g -filling and covalency. In summary, many metal oxides have abundant hydroxyls on the surface

and can depress the CO poisoning based on a bifunctional mechanism; they also have strong interaction with metal nanoparticles, which can not only realize the uniform dispersion of metal nanoparticles on supports, but also modify the electronic structure of metal nanocatalysts and thus improve their electrocatalytic performance by an electronic effect.

Among these studied metal oxides, some metal oxides are promising for PEFCs. First of all, Magnéti phase titanium oxides especially Ti_4O_7 because of their strong oxidation resistance are an excellent choice for PEFCs in long-time operation. As mentioned in Section 3.1.2, the Pt- TiO_x and Pt-Ti/ TiO_x catalysts exhibit 2-fold higher specific activity for ORR than Pt/Vulcan XC72 after the cyclic tests sweeping from 0.05 to 1.0 V. They retain their initial electrochemical active area even after 10,000 cycles between 1.0 and 1.5 V. Second, Nb- and Mo-doped TiO_2 are very helpful for the improvement in the activity of Pt catalysts. As mentioned in Section 3.1.3, the Pt/Nb- TiO_2 catalyst exhibits higher onset potentials (1.0 V) and mass activity of Pt ($235.3 \text{ mA mg}^{-1}@0.8 \text{ V}$) for ORR than those (0.9 V and $58.8 \text{ mA mg}^{-1}@0.8 \text{ V}$) of Pt/Vulcan XC-72, while the Pt/ $\text{Ti}_{0.7}\text{Mo}_{0.3}\text{O}_2$ exhibits not only 7 and 2.6 fold higher activity than the commercial Pt/C and PtCo/C catalysts. Third, tungsten oxides and molybdenum oxides demonstrate a huge potential in PEFCs because of the formation of hydrogen tungsten/molybdenum bronzes and the presence of hydrogen spillover effect. As shown in Section 3.2.3, the Pd- WO_3/C catalysts in a large range of WO_3 content between 10 wt% and 65 wt% exhibit much better catalytic activity and stability for FAOR than the Pd/C catalysts. Especially the one with WO_3 of 20 wt% has twice catalytic activity that of Pd/C catalyst. Last but not least, Perovskite oxides because of their flexible structure and variable valency are promising

to be developed as highly active non-noble-metal catalysts for PEFCs in alkaline. As shown in Section 3.8.2, the perovskite oxides such as $\text{LaMnO}_{3+\delta}$ and LaNiO_3 have intrinsic ORR activity in alkaline solution comparable to the state-of-the-art Pt/C (only ~ 50 mV shift corresponding to less than an order of activity difference). Undoubtedly, the use of non-noble metal catalysts will significantly reduce the cost of catalysts and thus the whole fuel cells.

Although some metal oxides have high electronic conductivity and stability, the present problems about most metal oxides are still low electronic conductivity, specific surface area and stability. Therefore, the future work can be focused on several aspects: doping with other metal ions to reduce the band gap and improve electronic conductivity; developing 3D hierarchical nanostructures to increase specific surface area; studying the interaction mechanism between metal and metal oxide, and modifying metal oxides to increase the interaction and thus chemical and electrochemical stability.

References

- 1 R. Borup, J. Meyers, B. Pivovar, Y. S. Kim, R. Mukundan, N. Garland, D. Myers, M. Wilson and F. Garzon, *Chem. Rev.*, 2007, **107**, 3904 .
- 2 M. K. Debe, *Nature*, 2012, **486**, 43.
- 3 V. Tripković, F. Abild-Pedersen, F. Studt, I. Cerri, T. Nagami, T. Bligaard and J. Rossmeisl, *ChemCatChem*, 2012, **4**, 228.
- 4 V. Di Noto, E. Negro, S. Polizzi, F. Agresti and G. A. Giffin, *ChemSusChem*, 2012, **5**, 2451.
- 5 V. Di Noto, E. Negro, S. Polizzi, P. Riello, and P. Atanassov, *Appl. Catal. B*, 2012, **185**, 111.
- 6 V. Di Noto, E. Negro, K. Vezzu, L. Toniolo and G. Pace, *Electrochim. Acta*, 2011, **57**, 257.
- 7 V. Di Noto and E. Negro, *Electrochim. Acta*, 2010, **55**, 1407.
- 8 K. W. Park, J. H. Choi, B. K. Kwon, S. A. Lee, Y. E. Sung, H. Y. Ha, S. A. Hong, H. Kim and A. Wieckowski, *J. Phys. Chem. B*, 2002, **106**, 1869.
- 9 M. Watanabe and S. Motoo, *J. Electroanal. Chem.*, 1975, **60**, 267.
- 10 J. L. Fernandez, D. A. Walsh and A. J. Bard, *J. Am. Chem. Soc.*, 2005, **127**, 357.
- 11 J. A. Farmer and C. T. Campbell, *Science*, 2010, **329**, 933.
- 12 Z. Chen, D. Higgins, A. Yu, L. Zhang and J. Zhang, *Energy Environ. Sci.*, 2011, **4**, 3167.
- 13 N. Zhang, S. Zhang, T. Zhu and G. Yin, *Prog. Chem.*, 2011, **23**, 2240.
- 14 J. E. Graves, D. Pletcher, R. L. Clarke and F. C. Walsh, *J. Appl. Electrochem.*, 1991, **21**, 848.

- 15 A. Fujishima and K. Honda, *Nature*, 1972, **238**, 37.
- 16 S. J. Tauster, S. C. Fung and R. L. Garten, *J. Am. Chem. Soc.*, 1978, **100**, 170.
- 17 B. Parkinson, F. Decker, J. F. Julião, M. Abramovich and H. C. Chagas, *Electrochim. Acta*, 1980, **25**, 521.
- 18 V. B. Baez, J. E. Graves and D. Pletcher, *J. Electroanal. Chem.*, 1992, **340**, 273.
- 19 J.-H. Kim, A. Ishihara, S. Mitsushima, N. Kamiya and K.-I. Ota, *Electrochim. Acta*, 2007, **52**, 2492.
- 20 M. Hepel, I. Dela, T. Hepel, J. Luo and C. J. Zhong, *Electrochim. Acta*, 2007, **52**, 5529.
- 21 M. Gustavsson, H. Ekström, P. Hanarp, L. Eurenus, G. Lindbergh, E. Olsson and B. Kasemo, *J. Power Sources*, 2007, **163**, 671.
- 22 N. Rajalakshmi, N. Lakshmi and K. S. Dhathathreyan, *Int. J. Hydrogen Energy*, 2008, **33**, 7521.
- 23 S.-Y. Huang, P. Ganesan, H.-Y. Jung and B. N. Popov, *J. Power Sources*, 2012, **198**, 23.
- 24 J. R. Smith, F. C. Walsh and R. L. Clarke, *J. Appl. Electrochem.*, 1998, **28**, 1021.
- 25 R. F. Bartholomew and D. R. Frankl, *Phys. Rev.*, 1969, **187**, 828.
- 26 G. Chen, S. R. Bare and T. E. Mallouk, *J. Electrochem. Soc.*, 2002, **149**, A1092.
- 27 T. Ioroi, Z. Siroma, N. Fujiwara, S.-i. Yamazaki and K. Yasuda, *Electrochem. Commun.*, 2005, **7**, 183.
- 28 T. Ioroi, H. Senoh, Z. Siroma, S.-i. Yamazaki, N. Fujiwara and K. Yasuda, *ECS Trans.*, 2007, **11**, 1041.

- 29 T. Ioroi, H. Senoh, S.-i. Yamazaki, Z. Siroma, N. Fujiwara and K. Yasuda, *J. Electrochem. Soc.*, 2008, **155**, B321.
- 30 T. Ioroi, T. Akita, S.-i. Yamazaki, Z. Siroma, N. Fujiwara and K. Yasuda, *J. Electrochem. Soc.*, 2011, **158**, C329.
- 31 T. Ioroi, T. Akita, M. Asahi, S.-i. Yamazaki, Z. Siroma, N. Fujiwara and K. Yasuda, *J. Power Sources*, 2013, **223**, 183.
- 32 L. Zhang, J. Kim, J. Zhang, F. Nan, N. Gauquelin, G. A. Botton, P. He, R. Bashyam and S. Knights, *Appl. Energy*, 2013, **103**, 507.
- 33 B. L. Garc ía, R. Fuentes and J. W. Weidner, *Electrochem. Solid-State Lett.*, 2007, **10**, B108.
- 34 K.-W. Park and K.-S. Seol, *Electrochem. Commun.*, 2007, **9**, 2256.
- 35 R. E. Fuentes, B. L. Garcia and J. W. Weidner, *ECS Trans.*, 2008, **12**, 239.
- 36 H. Chhina, S. Campbell and O. Kesler, *J. Electrochem. Soc.*, 2009, **156**, B1232.
- 37 S. L. Gojković, B. M. Babić, V. R. Radmilović and N. V. Krstajić, *J. Electroanal. Chem.*, 2010, **639**, 161.
- 38 O. E. Haas, S. T. Briskeby, O. E. Kongstein, M. Tsytkin, R. Tunold and B. T. Børresen, *J. New Mater. Electrochem. Syst.*, 2008, **11**, 9.
- 39 V. T. T. Ho, C.-J. Pan, J. Rick, W.-N. Su and B.-J. Hwang, *J. Am. Chem. Soc.*, 2011, **133**, 11716.
- 40 L. Xiong and A. Manthiram, *Electrochim. Acta*, 2004, **49**, 4163.
- 41 S. Shanmugam and A. Gedanken, *Small*, 2007, **3**, 1189.
- 42 A. Bauer, C. Song, A. Ignaszak, R. Hui, J. Zhang, L. Chevallier, D. Jones and J. Rozière, *Electrochim. Acta*, 2010, **55**, 8365.

- 43 J.-M. Chen, L. S. Sarma, C.-H. Chen, M.-Y. Cheng, S.-C. Shih, G.-R. Wang, D.-G. Liu, J.-F. Lee, M.-T. Tang and B.-J. Hwang, *J. Power Sources*, 2006, **159**, 29.
- 44 E. N. Muhamad, T. Takeguchi, G. Wang, Y. Anzai and W. Ueda, *J. Electrochem. Soc.*, 2009, **156**, B32.
- 45 G. Selvarani, S. Maheswari, P. Sridhar, S. Pitchumani and A. K. Shukla, *J. Electrochem. Soc.*, 2009, **156**, B1354.
- 46 X.-M. Wang, J. Wang, Q.-Q. Zou and Y.-Y. Xia, *Electrochim. Acta*, 2011, **56**, 1646.
- 47 W.-L. Qu, Z.-B. Wang, X.-L. Sui, D.-M. Gu and G.-P. Yin, *Int. J. Hydrogen Energy*, 2012, **37**, 15096.
- 48 H. Song, X. Qiu, F. Li, W. Zhu and L. Chen, *Electrochem. Commun.*, 2007, **9**, 1416.
- 49 N. G. Akalework, C.-J. Pan, W.-N. Su, J. Rick, M.-C. Tsai, J.-F. Lee, J.-M. Lin, L.-D. Tsai and B.-J. Hwang, *J. Mater. Chem.*, 2012, **22**, 20977.
- 50 O. K. Varghese, M. Paulose and C. A. Grimes, *Nat. Nanotechnol.*, 2009, **4**, 592.
- 51 H. Song, X. Qiu, X. Li, F. Li, W. Zhu and L. Chen, *J. Power Sources*, 2007, **170**, 50.
- 52 H. Song, X. Qiu, D. Guo and F. Li, *J. Power Sources*, 2008, **178**, 97.
- 53 J. M. Macak, F. Schmidt-Stein and P. Schmuki, *Electrochem. Commun.*, 2007, **9**, 1783.
- 54 D.-H. Lim, W.-J. Lee, J. Wheldon, N. L. Macy and W. H. Smyrl, *J. Electrochem. Soc.*, 2010, **157**, B862.

- 55 T. Maiyalagan, B. Viswanathan and U. V. Varadaraju, *J. Nanosci. Nanotechnol.*, 2006, **6**, 2067.
- 56 Q.-Z. Jiang, X. Wu, M. Shen, Z.-F. Ma and X.-Y. Zhu, *Catal. Lett.*, 2008, **124**, 434.
- 57 R. E. Rettew, N. K. Allam and F. M. Alamgir, *ACS Appl. Mater. Inter.*, 2011, **3**, 147.
- 58 X. Guo, D.-J. Guo, X.-P. Qiu, L.-Q. Chen and W.-T. Zhu, *J. Power Sources*, 2009, **194**, 281.
- 59 X. He and C. Hu, *J. Power Sources*, 2011, **196**, 3119.
- 60 Q. Long, M. Cai, J. Li, H. Rong and L. Jiang, *J. Nanopart. Res.*, 2011, **13**, 1655.
- 61 T. Saida, N. Ogiwara, Y. Takasu and W. Sugimoto, *J. Phys. Chem. C*, 2010, **114**, 13390.
- 62 O. Micic, Y. Zhang, K. R. Cromack, A. Trifunac and M. Thurnauer, *J. Phys. Chem.*, 1993, **97**, 13284.
- 63 P. A. Mandelbaum, A. E. Regazzoni, M. A. Blesa and S. A. Bilmes, *J. Phys. Chem. B*, 1999, **103**, 5505.
- 64 K. Drew, G. Girishkumar, K. Vinodgopal and P. V. Kamat, *J. Phys. Chem. B*, 2005, **109**, 11851.
- 65 C. Jia, H. Yin, H. Ma, R. Wang, X. Ge, A. Zhou, X. Xu and Y. Ding, *J. Phys. Chem. C*, 2009, **113**, 16138.
- 66 Y. Q. Wang, Z. D. Wei, B. Gao, X. Q. Qi, L. Li, Q. Zhang and M. R. Xia, *J. Power Sources*, 2011, **196**, 1132.
- 67 J. E. Benson, H. W. Kohn and M. Boudart, *J. Catal.*, 1966, **5**, 307.

- 68 B. S. Hobbs and A. C. C. Tseung, *Nature*, 1969, **222**, 556.
- 69 K. Y. Chen, P. K. Shen and A. C. C. Tseung, *J. Electrochem. Soc.*, 1995, **142**, L185.
- 70 P. K. Shen, K. Y. Chen and A. C. C. Tseung, *J. Electrochem. Soc.*, 1995, **142**, L85.
- 71 P. K. Shen, K. Y. Chen and A. C. C. Tseung, *J. Chem. Soc., Faraday Trans.*, 1994, **90**, 3089.
- 72 K. Y. Chen, P. K. Shen and A. C. C. Tseung, *J. Electrochem. Soc.*, 1995, **142**, L54.
- 73 G. Lalande, M. C. Denis, P. Gouérec, D. Guay, J. P. Dodelet and R. Schulz, *J. New Mater. Electrochem. Syst.*, 2000, **3**, 185.
- 74 C. H. Lee, C. W. Lee, D. H. Jung, C. S. Kim and D. R. Shin, *J. New Mater. Electrochem. Syst.*, 1999, **2**, 125.
- 75 F. Shafia Hoor, M. F. Ahmed and S. M. Mayanna, *J. Solid State Electrochem.*, 2004, **8**, 572.
- 76 K.-W. Park, K.-S. Ahn, J.-H. Choi, Y.-C. Nah and Y.-E. Sung, *Appl. Phys. Lett.*, 2003, **82**, 1090.
- 77 K.-W. Park, Y.-W. Lee and Y.-E. Sung, *Appl. Catal. B*, 2013, **132–133**, 237.
- 78 P. M. S. Monk, R. D. Partridge, R. Janes and M. J. Parker, *J. Mater. Chem.*, 1994, **4**, 1071.
- 79 V. Raghuvver and B. Viswanathan, *J. Power Sources*, 2005, **144**, 1.
- 80 M. Nagarajan, G. Paruthimal Kalaigan and G. A. Pathanjali, *Ionics*, 2013, **19**, 127.

- 81 Z. Zhang, Y. Huang, J. Ge, C. Liu, T. Lu and W. Xing, *Electrochem. Commun.*, 2008, **10**, 1113.
- 82 Z. Zhang, X. Wang, Z. Cui, C. Liu, T. Lu and W. Xing, *J. Power Sources*, 2008, **185**, 941.
- 83 L. G. S. Pereira, F. R. dos Santos, M. E. Pereira, V. A. Paganin and E. A. Ticianelli, *Electrochim. Acta*, 2006, **51**, 4061.
- 84 F. Maillard, E. Peyrelade, Y. Soldo-Olivier, M. Chatenet, E. Chañet and R. Faure, *Electrochim. Acta*, 2007, **52**, 1958.
- 85 C. Roth, M. Goetz and H. Fuess, *J. Appl. Electrochem.*, 2001, **31**, 793.
- 86 D. Y. Zhang, Z. F. Ma, G. X. Wang, K. Konstantinov, X. X. Yuan and H. K. Liu, *Electrochem. Solid-State Lett.*, 2006, **9**, A423.
- 87 K. Miecznikowski and P. J. Kulesza, *J. Power Sources*, 2011, **196**, 2595.
- 88 B. Rajesh, V. Karthik, S. Karthikeyan, K. Ravindranathan Thampi, J. M. Bonard and B. Viswanathan, *Fuel*, 2002, **81**, 2177.
- 89 E. Kang, S. An, S. Yoon, J. K. Kim and J. Lee, *J. Mater. Chem.*, 2010, **20**, 7416.
- 90 X. Cui, L. Guo, F. Cui, Q. He and J. Shi, *J. Phys. Chem. C*, 2009, **113**, 4134.
- 91 M. Dou, M. Hou, H. Zhang, G. Li, W. Lu, Z. Wei, Z. Shao and B. Yi, *ChemSusChem*, 2012, **5**, 945.
- 92 X. Cui, Z. Hua, C. Wei, Z. Shu, L. Zhang, H. Chen and J. Shi, *Chem. Asian J.*, 2013, **8**, 429.
- 93 R. Ganesan and J. S. Lee, *J. Power Sources*, 2006, **157**, 217.
- 94 T. Maiyalagan and B. Viswanathan, *J. Power Sources*, 2008, **175**, 789.

- 95 J. Zhang, J.-p. Tu, G.-h. Du, Z.-m. Dong, Q.-m. Su, D. Xie and X.-l. Wang, *Electrochim. Acta*, 2013, **88**, 107.
- 96 Z. Yan, W. Wei, J. Xie, S. Meng, X. Lü and J. Zhu, *J. Power Sources*, 2013, **222**, 218.
- 97 J. Horkans and M. W. Shafer, *J. Electrochem. Soc.*, 1977, **124**, 1196.
- 98 Z. Yan, J. Xie, J. Jing, M. Zhang, W. Wei and S. Yin, *Int. J. Hydrogen Energy*, 2012, **37**, 15948.
- 99 L. Chen, A. C. Cooper, G. P. Pez and H. Cheng, *J. Phys. Chem. C*, 2008, **112**, 1755.
- 100 P. Justin and G. Ranga Rao, *Int. J. Hydrogen Energy*, 2011, **36**, 5875.
- 101 O. Guillén-Villafuerte, G. García, R. Guil-López, E. Nieto, J. L. Rodríguez, J. L. G. Fierro and E. Pastor, *J. Power Sources*, 2013, **231**, 163.
- 102 Y. Wang, E. R. Fachini, G. Cruz, Y. Zhu, Y. Ishikawa, J. A. Colucci and C. R. Cabrera, *J. Electrochem. Soc.*, 2001, **148**, C222.
- 103 N. R. Elezović, B. M. Babić, V. R. Radmilović, S. L. Gojković, N. V. Krstajić and L. M. Vračar, *J. Power Sources*, 2008, **175**, 250.
- 104 E. N. Muhamad, T. Takeguchi, F. Wang, G. Wang, T. Yamanaka and W. Ueda, *J. Electrochem. Soc.*, 2009, **156**, B1361.
- 105 N. Tsiouvaras, M. V. Martínez-Huerta, R. Moliner, M. J. Lázaro, J. L. Rodríguez, E. Pastor, M. A. Peña and J. L. G. Fierro, *J. Power Sources*, 2009, **186**, 299.
- 106 Z. Liu, J. E. Hu, Q. Wang, K. Gaskell, A. I. Frenkel, G. S. Jackson and B. Eichhorn, *J. Am. Chem. Soc.*, 2009, **131**, 6924.

- 107 F. Alcaide, G. Álvarez, N. Tsiouvaras, M. A. Peña, J. L. G. Fierro and M. V. Martínez-Huerta, *Int. J. Hydrogen Energy*, 2011, **36**, 14590.
- 108 Z. Hou, B. Yi, H. Yu, Z. Lin and H. Zhang, *J. Power Sources*, **2003**, 123, 116.
- 109 Z. H. Zhou, W. S. Li, Z. Fu and X. D. Xiang, *Int. J. Hydrogen Energy*, 2010, **35**, 936.
- 110 W. Li, J. Lu, J. Du, D. Lu, H. Chen, H. Li and Y. Wu, *Electrochem. Commun.*, 2005, **7**, 406.
- 111 H. B. Suffredini, V. Tricoli, L. A. Avaca and N. Vattistas, *Electrochem. Commun.*, 2004, **6**, 1025.
- 112 K. Lasch, G. Hayn, L. Jörisen, J. Garche and O. Besenhardt, *J. Power Sources*, 2002, **105**, 305.
- 113 F. Peng, C. Zhou, H. Wang, H. Yu, J. Liang and J. Yang, *Catal. Commun.*, 2009, **10**, 533.
- 114 S. Pylypenko, B. B. Blizanac, T. S. Olson, D. Konopka and P. Atanassov, *ACS Appl. Mater. Inter.*, 2009, **1**, 604.
- 115 D. A. McKeown, P. L. Hagans, L. P. L. Carette, A. E. Russell, K. E. Swider and D. R. Rolison, *J. Phys. Chem. B*, 1999, **103**, 4825.
- 116 W. Dmowski, T. Egami, K. E. Swider-Lyons, C. T. Love and D. R. Rolison, *J. Phys. Chem. B*, 2002, **106**, 12677.
- 117 D. R. Rolison, P. L. Hagans, K. E. Swider and J. W. Long, *Langmuir*, 1999, **15**, 774.
- 118 J. W. Long, R. M. Stroud, K. E. Swider-Lyons and D. R. Rolison, *J. Phys. Chem. B*, 2000, **104**, 9772.

- 119 Z. Chen, X. Qiu, B. Lu, S. Zhang, W. Zhu and L. Chen, *Electrochem. Commun.*, 2005, **7**, 593.
- 120 F. Scheiba, M. Scholz, L. Cao, R. Schafranek, C. Roth, C. Cremers, X. Qiu, U. Stimming and H. Fuess, *Fuel Cells*, 2006, **6**, 439.
- 121 S. V. Selvaganesh, G. Selvarani, P. Sridhar, S. Pitchumani and A. K. Shukla, *J. Electrochem. Soc.*, 2012, **159**, B463.
- 122 C. Zhou, F. Peng, H. Wang, H. Yu, J. Yang and X. Fu, *Fuel Cells*, 2011, **11**, 301.
- 123 C.-P. Lo and V. Ramani, *ACS Appl. Mater. Inter.*, 2012, **4**, 6109.
- 124 L. Zheng, Q. Zeng, S. Liao and J. Zeng, *Int. J. Hydrogen Energy*, 2012, **37**, 13103.
- 125 S. Wendt, M. Knapp and H. Over, *J. Am. Chem. Soc.*, 2004, **126**, 1537.
- 126 Y.-J. Gu and W.-T. Wong, *J. Electrochem. Soc.*, 2006, **153**, A1714.
- 127 T. Saida, W. Sugimoto and Y. Takasu, *Electrochim. Acta*, 2010, **55**, 857.
- 128 Z. Zhang, J. Ge, L. Ma, J. Liao, T. Lu and W. Xing, *Fuel Cells*, 2009, **9**, 114.
- 129 F. Ye, J. Li, T. Wang, Y. Liu, H. Wei, J. Li and X. Wang, *J. Phys. Chem. C*, 2008, **112**, 12894.
- 130 K. Waki, K. Matsubara, K. Ke and Y. Yamazaki, *Electrochem. Solid-State Lett.*, 2005, **8**, A489.
- 131 T. Matsui, K. Fujiwara, T. Okanishi, R. Kikuchi, T. Takeguchi and K. Eguchi, *J. Power Sources*, 2006, **155**, 152.
- 132 A. Sandoval-González, E. Borja-Arco, J. Escalante, O. Jiménez-Sandoval and S. A. Gamboa, *Int. J. Hydrogen Energy*, 2012, **37**, 1752.
- 133 L. Jiang, G. Sun, Z. Zhou, S. Sun, Q. Wang, S. Yan, H. Li, J. Tian, J. Guo, B. Zhou and Q. Xin, *J. Phys. Chem. B*, 2005, **109**, 8774.

- 134 L. Jiang, L. Colmenares, Z. Jusys, G. Q. Sun and R. J. Behm, *Electrochim. Acta*, 2007, **53**, 377.
- 135 D. F. Silva, A. N. Geraldes, A. O. Neto, E. S. Pino, M. Linardi, E. V. Spinacé W. A. A. Macedo and J. D. Ardisson, *Mater. Sci. Eng. B*, 2010, **175**, 261.
- 136 A. Kowal, M. Li, M. Shao, K. Sasaki, M. B. Vukmirovic, J. Zhang, N. S. Marinkovic, P. Liu, A. I. Frenkel and R. R. Adzic, *Nat. Mater.*, 2009, **8**, 325.
- 137 A. Kowal, S. L. Gojković, K. S. Lee, P. Olszewski and Y. E. Sung, *Electrochem. Commun.*, 2009, **11**, 724.
- 138 K.-S. Lee, I.-S. Park, Y.-H. Cho, D.-S. Jung, N. Jung, H.-Y. Park and Y.-E. Sung, *J. Catal.*, 2008, **258**, 143.
- 139 A. Oliveira Neto, M. Brandalise, R. R. Dias, J. M. S. Ayoub, A. C. Silva, J. C. Penteado, M. Linardi and E. V. Spinacé *Int. J. Hydrogen Energy*, 2010, **35**, 9177.
- 140 F. Takasaki, Z. Noda, A. Masao, Y. Shiratori, K. Ito and K. Sasaki, *ECS Trans.*, 2009, **25**, 831.
- 141 M. S. Saha, R. Li, M. Cai and X. Sun, *Electrochem. Solid-State Lett.*, 2007, **10**, B130.
- 142 M. S. Saha, R. Li and X. Sun, *Electrochem. Commun.*, 2007, **9**, 2229.
- 143 A. B. Suryamas, G. M. Anilkumar, S. Sago, T. Ogi and K. Okuyama, *Catal. Commun.*, 2013, **33**, 11.
- 144 M. Dou, M. Hou, D. Liang, W. Lu, Z. Shao, B. Yi, *Electrochim. Acta*, 2013, **92**, 468.
- 145 P. Zhang, S.-Y. Huang and B. N. Popov, *J. Electrochem. Soc.*, 2010, **157**, B1163.
- 146 C. Sun, H. Li and L. Chen, *Energy Environ. Sci.*, 2012, **5**, 8475.

- 147 P. Jasinski, T. Suzuki and H. U. Anderson, *Sensor Actuat. B-Chem*, 2003, **95**, 73.
- 148 Z. Zhang, H. Gao, W. Cai, C. Liu, Y. Guo and P.-X. Gao, *J. Mater. Chem.*, 2012, **22**, 23098.
- 149 K. Kuwaha and A. Matsuoka, *Japan Pat.*, 10-55807, 1998.
- 150 H. B. Yu, J.-H. Kim, H.-I. Lee, M. A. Scibioh, J. Lee, J. Han, S. P. Yoon and H. Y. Ha, *J. Power Sources*, 2005, **140**, 59.
- 151 H. Xu and X. Hou, *Int. J. Hydrogen Energy*, 2007, **32**, 4397.
- 152 K. H. Lee, K. Kwon, V. Roev, D. Y. Yoo, H. Chang and D. Seung, *J. Power Sources*, 2008, **185**, 871.
- 153 C. Xu and P. K. Shen, *Chem. Commun.*, 2004, 2238.
- 154 C. Xu, R. Zeng, P. K. Shen and Z. Wei, *Electrochim. Acta*, 2005, **51**, 1031.
- 155 C. Xu, P. k. Shen and Y. Liu, *J. Power Sources*, 2007, **164**, 527.
- 156 A. O. Neto, L. A. Farias, R. R. Dias, M. Brandalise, M. Linardi and E. V. Spinac é *Electrochem. Commun.*, 2008, **10**, 1315.
- 157 A. Neto, M. Linardi, D. Anjos, G. Tremiliosi-Filho and E. Spinac é *J. Appl. Electrochem.*, 2009, **39**, 1153.
- 158 L. Yu and J. Xi, *Int. J. Hydrogen Energy*, 2012, **37**, 15938.
- 159 M. Takahashi, T. Mori, F. Ye, A. Vinu, H. Kobayashi and J. Drennan, *J. Am. Ceram. Soc.*, 2007, **90**, 1291.
- 160 M. A. Scibioh, S.-K. Kim, E. A. Cho, T.-H. Lim, S.-A. Hong and H. Y. Ha, *Appl. Catal. B*, 2008, **84**, 773.
- 161 D. R. Ou, T. Mori, H. Togasaki, M. Takahashi, F. Ye and J. Drennan, *Langmuir*, 2011, **27**, 3859.

- 162 Z. Xu, Z. Qi and A. Kaufman, *J. Power Sources*, 2003, **115**, 40.
- 163 Y. Bai, J. Wu, X. Qiu, J. Xi, J. Wang, J. Li, W. Zhu and L. Chen, *Appl. Catal. B*, 2007, **73**, 144.
- 164 B. Choi, J. Prabhuram, M. A. Scibioh, H.-I. Joh, Y.-E. Sung, H. Y. Ha and S.-K. Kim, *J. Electrochem. Soc.*, 2009, **156**, B801.
- 165 J. P. Brenet, *J. Power Sources*, 1979, **4**, 183.
- 166 F. H. B. Lima, M. L. Calegario and E. A. Ticianelli, *J. Electroanal. Chem.*, 2006, **590**, 152.
- 167 F. H. B. Lima, M. L. Calegario and E. A. Ticianelli, *Electrochim. Acta*, 2007, **52**, 3732.
- 168 Y. Zhao, L. Zhan, J. Tian, S. Nie and Z. Ning, *Int. J. Hydrogen Energy*, 2010, **35**, 10522.
- 169 F. Cheng, Y. Su, J. Liang, Z. Tao and J. Chen, *Chem. Mater.*, 2010, **22**, 898.
- 170 F. Cheng, T. Zhang, Y. Zhang, J. Du, X. Han and J. Chen, *Angew. Chem. Int. Ed.*, 2013, **52**, 2474.
- 171 L. Mao, T. Sotomura, K. Nakatsu, N. Koshiba, D. Zhang and T. Ohsaka, *J. Electrochem. Soc.*, 2002, **149**, A504.
- 172 T. Ohsaka, L. Mao, K. Arihara and T. Sotomura, *Electrochem. Commun.*, 2004, **6**, 273.
- 173 M. S. El-Deab and T. Ohsaka, *Angew. Chem. Int. Ed.*, 2006, **45**, 5963.
- 174 Y. Gorlin and T. F. Jaramillo, *J. Am. Chem. Soc.*, 2010, **132**, 13612.
- 175 K. W. Kim, S. M. Kim, S. Choi, J. Kim and I. S. Lee, *ACS Nano*, 2012, **6**, 5122.

- 176 Y. Gorlin, C.-J. Chung, D. Nordlund, B. M. Clemens and T. F. Jaramillo, *ACS Catal.*, 2012, **2**, 2687.
- 177 Y. Tan, C. Xu, G. Chen, X. Fang, N. Zheng and Q. Xie, *Adv. Funct. Mater.*, 2012, **22**, 4584.
- 178 J. Yang and J. J. Xu, *Electrochem. Commun.*, 2003, **5**, 306.
- 179 J. S. Rebello, P. V. Samant, J. L. Figueiredo and J. B. Fernandes, *J. Power Sources*, 2006, **153**, 36.
- 180 N. Ohno, Y. Akeboshi, M. Saito, J. Kuwano, H. Shiroishi, T. Okumura and Y. Uchimoto, *Top. Catal.*, 2009, **52**, 903.
- 181 M. S. El-Deab, *J. Adv. Res.*, 2010, **1**, 87.
- 182 W. Sun, A. Hsu and R. Chen, *J. Power Sources*, 2011, **196**, 4491.
- 183 H. Tanaka and M. Misono, *Curr. Opin. Solid State Mater. Sci.*, 2001, **5**, 381.
- 184 Y. Nishihata, J. Mizuki, T. Akao, H. Tanaka, M. Uenishi, M. Kimura, T. Okamoto and N. Hamada, *Nature*, 2002, **418**, 164.
- 185 M. Ghasdi and H. Alamdari, *Sensor Actuat. B-Chem*, 2010, **148**, 478.
- 186 I. Z. Rahman, M. A. Raza and M. A. Rahman, *Adv. Mater. Res.*, 2012, **445**, 497.
- 187 J. O. M. Bockris and T. Otagawa, *J. Electrochem. Soc.*, 1984, **131**, 290.
- 188 A. Hammouche, A. Kahoul, D. U. Sauer and R. W. De Doncker, *J. Power Sources*, 2006, **153**, 239.
- 189 J. Tulloch and S. W. Donne, *J. Power Sources*, 2009, **188**, 359.
- 190 J. Suntivich, H. A. Gasteiger, N. Yabuuchi and Y. Shao-Horn, *J. Electrochem. Soc.*, 2010, **157**, B1263.

- 191 J. Sunarso, A. A. J. Torriero, W. Zhou, P. C. Howlett and M. Forsyth, *J. Phys. Chem. C*, 2012, **116**, 5827.
- 192 Y. Wang and H.-P. Cheng, *J. Phys. Chem. C*, 2013, **117**, 2106.
- 193 R. N. Singh, M. Malviya, Anindita, A. S. K. Sinha and P. Chartier, *Electrochim. Acta*, 2007, **52**, 4264.
- 194 T. Poux, F. S. Napolskiy, T. Dintzer, G. Kérangu éven, S. Y. Istomin, G. A. Tsirlina, E. V. Antipov and E. R. Savinova, *Catal. Today*, 2012, **189**, 83.
- 195 J. Suntivich, H. A. Gasteiger, N. Yabuuchi, H. Nakanishi, J. B. Goodenough and Y. Shao-Horn, *Nat. Chem.*, 2011, **3**, 546.

Figure Captions

Figure 1. Electron density surfaces ($\rho = 0.02$) with mapped electrostatic potential for $(\text{TiO}_2)_6$ super cells interacting with a single Pt ad-atom [20]: (a) after equilibration but without any bond formation, (b) with Pt bonded through O atoms to TiO_2 units and (c) with Pt bonded directly to Ti. Reproduced with permission of Elsevier.

Figure 2. Cyclic voltammograms of MEAs with (a) 20 wt% Pt-Ti/ TiO_x and (b) 40 wt% Pt/XC72 cathodes at 80 °C under N_2 flow conditions at the initial state, and after 5,000/10,000 potential sweep cycles [31]. Potential sweep: 1.0 - 1.5 V vs. anode; 500 mV s^{-1} . Reproduced with permission of Elsevier.

Figure 3. Polarization curves of (a) Vulcan XC72 and (b) Nb/ TiO_2 supported Pt cathode catalysts in oxygen-saturated 0.5 M H_2SO_4 at different rotation rates from 100 to 3600 rpm with a scan rate of 10 mV s^{-1} at 25 °C; (c) Comparison of catalytic activity for oxygen reduction on Vulcan XC72- and Nb/ TiO_2 -supported Pt cathode catalysts [34]. [The insets (a) and (b) are cyclic voltammograms of Vulcan XC72- and Nb/ TiO_2 -supported Pt cathode catalysts in 0.5 M H_2SO_4 , respectively.] Reproduced with permission of Elsevier.

Figure 4. (A) Pt L_{III} -edge XANES spectra and (B) variation in unfilled d-states for Pt foil and different catalyst samples (denoted in the Figure) [39]. (Inset) Enlarged region of peaks of Pt L_{III} -edge XANES white line. Reproduced with permission of the American Chemical Society (ACS).

Figure 5. Schematic presentations of the structures of Johnson-Matthey 30, E-TEK 30 Pt-Ru/C catalysts, and in-house prepared Pt-Ru/C and Pt-Ru-Ti/C catalysts [43]. Note: 30

means 20 wt% Pt and 10 wt% Ru; the provenance of the commercial products is described in the text. Reproduced with permission of Elsevier.

Figure 6. (a) Pt L_{III}-edge XANES spectra (inset shows an enlarged region of peaks of the Pt L_{III}-edge XANES white line); (b) calculated unfilled d-states for Pt foil and different catalyst samples (denoted in the Figure); (c) XAS spectra of Ti L_{II, III}-edge (inset shows an enlarged region of peaks) [49]. Reproduced with permission of the Royal Society of Chemistry.

Figure 7. XPS spectra of platinized TiO₂ nanotube electrodes. Lines indicate location of peaks for Pt reference foil [57]. Reproduced with permission of the ACS.

Figure 8. Left: Air breathing DMFC cell equipped with quartz window for UV excitation. Right: Galvanostatic polarization and power output data at 295 K using TiO₂/CFE/Pt-Ru anode and CFE/Pt black cathode (CFE = carbon fiber electrode) [64]. Traces were recorded (a) and (a') in the absence and (b) and (b') in the presence of UV illumination. The Pt loadings for both cathode and anode were 0.15 mg cm⁻² and TiO₂ loading of 0.4 mg cm⁻². Reproduced with permission of the ACS.

Figure 9. Schematic illustration of a possible mechanism for methanol photoelectrocatalysis on a TiO₂/nanoporous gold electrode under UV illumination [65]. Reproduced with permission of the ACS.

Figure 10. (a) Cyclic voltammograms of the Pd-WO₃/C catalysts in 0.5 M H₂SO₄ containing 0.5 M formic acid with a scan rate of 20 mV s⁻¹; (b) relationship between the specific activity and WO₃ content [81]. The specific activity was obtained from the current density of anode peaks for formic acid electrooxidation on Pd-WO₃/C catalysts. Reproduced with permission of Elsevier.

Figure 11. (a) CV scans of MoO_x/Pt core-shell and $\text{Pt}_{0.8}\text{Mo}_{0.2}$ alloy catalysts in 0.5 M H_2SO_4 at 298 K. (b) Polarization curves for oxidation of H_2 in the presence of 1000 ppm of CO on different catalysts (30% loading) at 298 K [106]. Rotation rate: 1600 rpm. Reproduced with permission of the ACS.

Figure 12. Current-potential and current-time polarization curves comparing the activity of $\text{PtRhSnO}_2/\text{C}$ with several other catalysts for ethanol oxidation [136]. (a) Polarization curves for ethanol oxidation on $\text{PtRhSnO}_2/\text{C}$ and PtSnO_2/C thin-film electrocatalysts deposited on glassy carbon electrodes in 0.1 M HClO_4 + 0.2 M ethanol. (b) Quasi-steady-state polarization curves for ethanol oxidation on $\text{PtRhSnO}_2/\text{C}$ and 20 wt% E-TEK Pt/C on glassy carbon electrodes. (c) Polarization curves for ethanol oxidation on $\text{PtRhSnO}_2/\text{C}$ and 20 wt% E-TEK 1:1 atomic PtRu on C at 60 °C. (d) Chronoamperometric measurements of ethanol oxidation at 0.45 V on $\text{PtRhSnO}_2/\text{C}$ and Pt/C catalysts at 60 °C for 0.5 M $\text{C}_2\text{H}_5\text{OH}$ in 0.1 M HClO_4 . The Pt/C current is multiplied by 40. Reproduced with permission of Nature.

Figure 13. Reorganized EELS spectra of $\text{Pt-CeO}_2/\text{C}$ catalysts and as-prepared CeO_2 [161]. (a) the Ce $\text{M}_{4,5}$ edge; (b) the Pt $\text{N}_{6,7}$ edge and Pt $\text{O}_{2,3}$ edge. Reproduced with permission of the ACS.

Figure 14. XPS spectra of (A) Pt4f, (B) Mn2p, and (C) O1s obtained for (a) bare Pt, and (b,c) nano- MnO_x/Pt electrodes [173]. MnO_x is prepared by electrodeposition after (b) 25 and (c) 100 potential cycles. The dotted lines in A and B corresponds to the binding energies of $4f_{7/2}$ and $4f_{5/2}$ of elemental Pt and $2p_{1/2}$ and $2p_{3/2}$ of elemental Mn, respectively. (D) Illustrates the proposed adsorption modes of molecular oxygen (small

white circles) at the Pt surface (large yellow circles) in the absence (Case I) and presence (Case II) of nano-MnO_x (black circles). Reproduced with permission of Wiley.

Figure 15. Oxygen electrode activities of the nanostructured Mn oxide thin film, nanoparticles of Pt, Ir, and Ru, and the GC substrate [174]. The Mn oxide thin film shows excellent activity for both the ORR and the OER. The CVs were measured with a sweep rate of 5 mV s⁻¹ in O₂ saturated 0.1 M KOH electrolyte at 23 °C. Reproduced with permission of the ACS.

Figure 16. (a) CVs of six samples: MnO/GC, MnO/pGC, Mn₃O₄/pGC, bare GC, bare pGC, and nanoparticulate Pt/C, all measured in oxygen saturated 0.1 M KOH electrolyte, at a 20 mV s⁻¹ sweep rate and 1600 rpm rotation rate. (b) Koutecky-Levich analysis of Mn₃O₄/pGC and Pt/C. (c) Tafel plots of kinetic current for MnO/pGC, Mn₃O₄/pGC, and Pt/C constructed after correcting the potential for uncompensated ohmic losses and capacitive current obtained in N₂ scans and removing mass-transport losses from the measured current. (d) Normalization of Tafel plots by estimated surface areas of Mn₃O₄ and Pt to determine specific activities of the catalysts as a function of applied potential [176]. Reproduced with permission of the ACS.

Figure 17. (a) ORR polarization curves for MnO-m-N-C, m-N-C, MnO, Pt/C, and physical mixture of m-N-C and MnO catalysts recorded in an O₂-saturated 0.1 M KOH aqueous solution at a sweep rate of 5 mV s⁻¹ at a rotation rate of 1,600 rpm. (b) Half-wave potentials (E_{1/2}) of these catalysts. (c) ORR-polarization curves for MnO-m-N-C catalyst at the different rotation rates. (d) Koutecky-Levich plots for MnO-m-N-C catalyst at different potentials [177]. Reproduced with permission of Wiley.

Figure 18. Structure of Perovskite (ABO_3) [183]. Black ball: A-site; Dark ball: B-site; White ball: Oxide ion. Reproduced with permission of Elsevier.

Figure 19. Role of e_g electron on ORR activity of perovskite oxides [195]. (a) Potentials at $25 \mu A cm_{ox}^{-2}$ as a function of e_g orbital in perovskite-based oxides. Data symbols vary with type of B ions (Cr, red; Mn, orange; Fe, grey; Co, green; Ni, blue; mixed compounds, purple), where $x = 0$ and 0.5 for Cr, and $0, 0.25$ and 0.5 for Fe. (b) The shape of the e_g electron points directly towards the surface O atom and plays an important role during O_2^{2-}/OH^- exchange. O, B and H atoms are colored red, blue and green, respectively. Reproduced with permission of Nature.

Figure 1

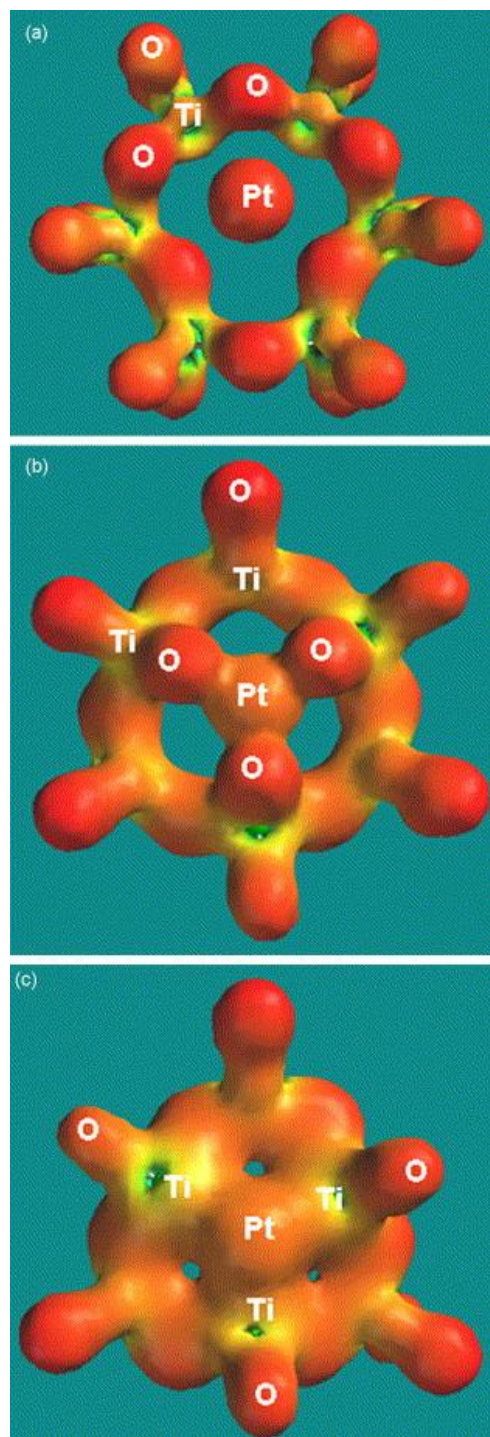


Figure 2

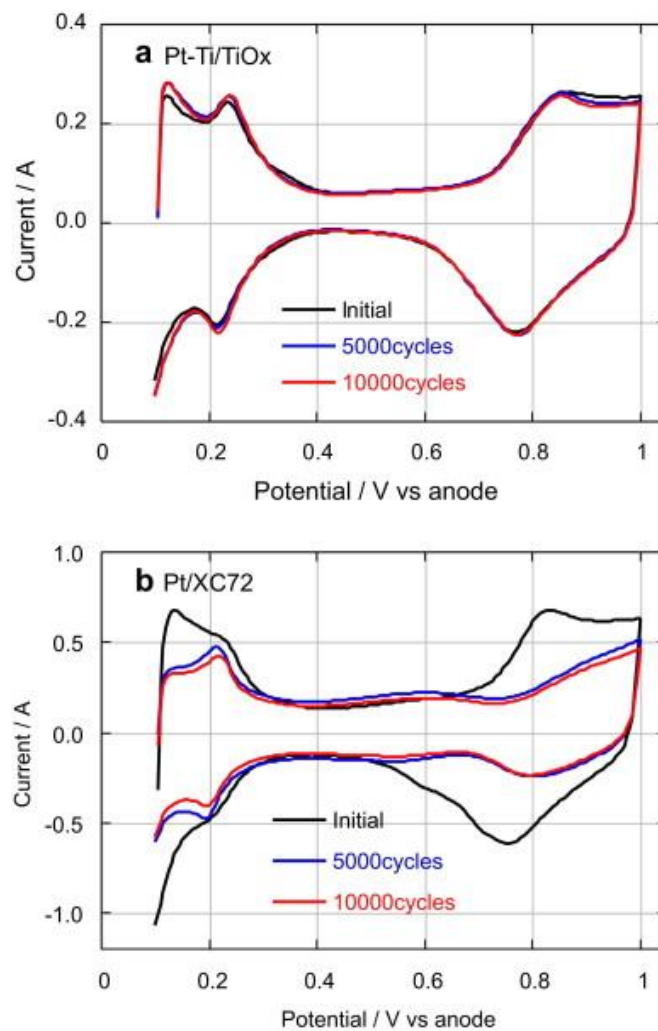


Figure 3

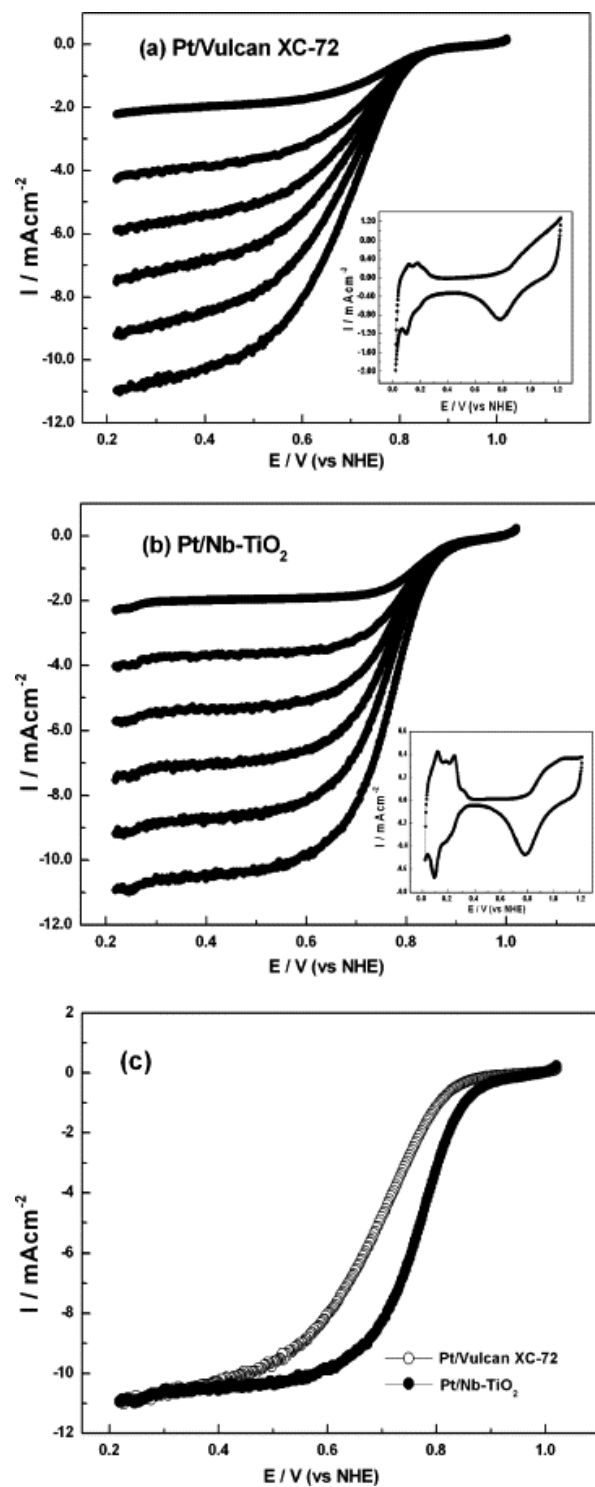


Figure 4

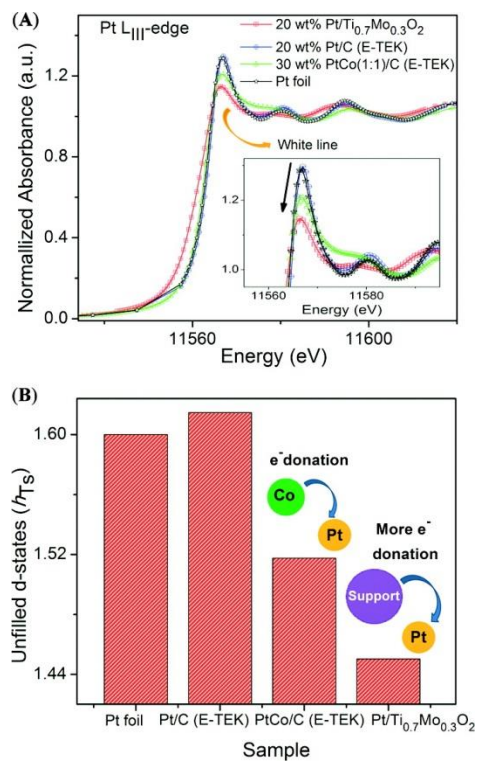


Figure 5

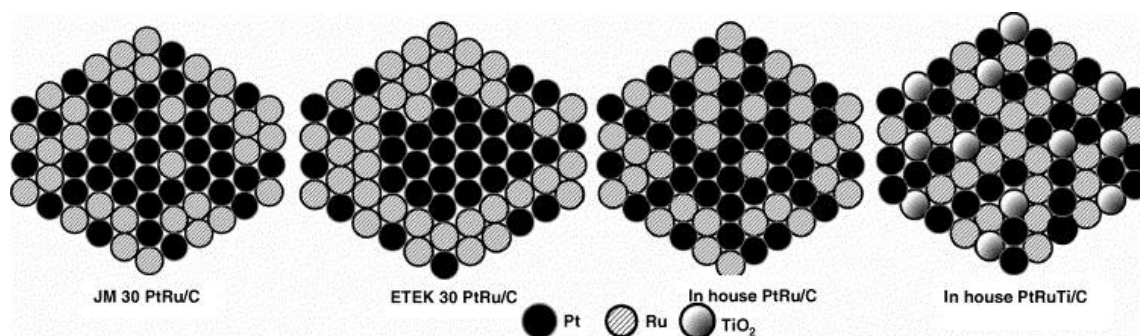


Figure 6

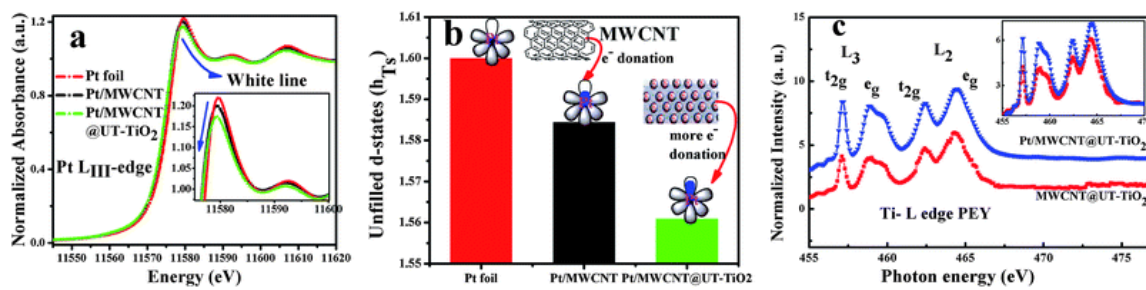


Figure 7

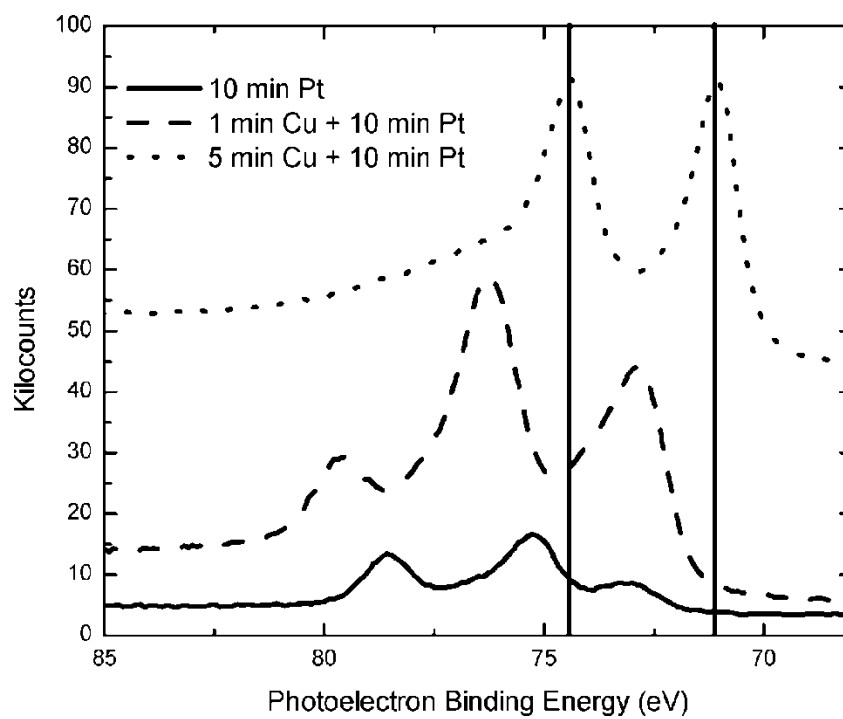


Figure 8

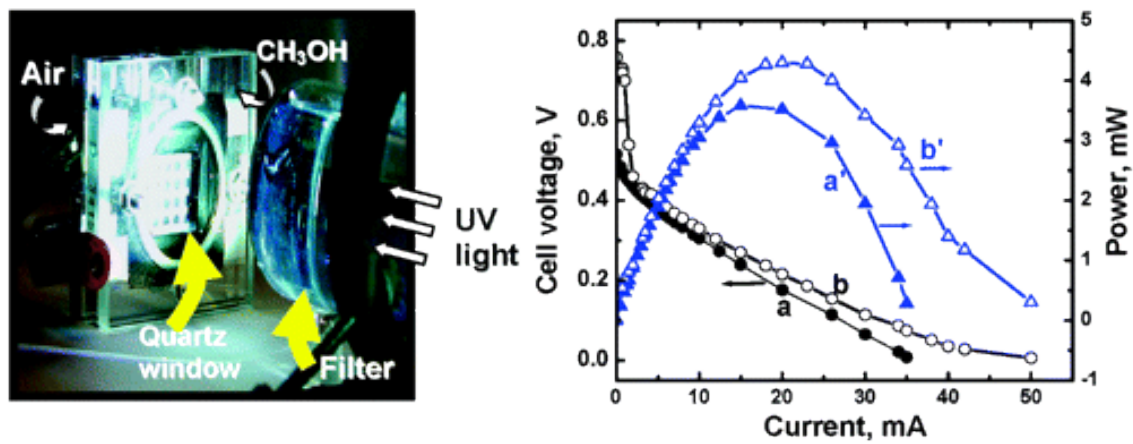


Figure 9

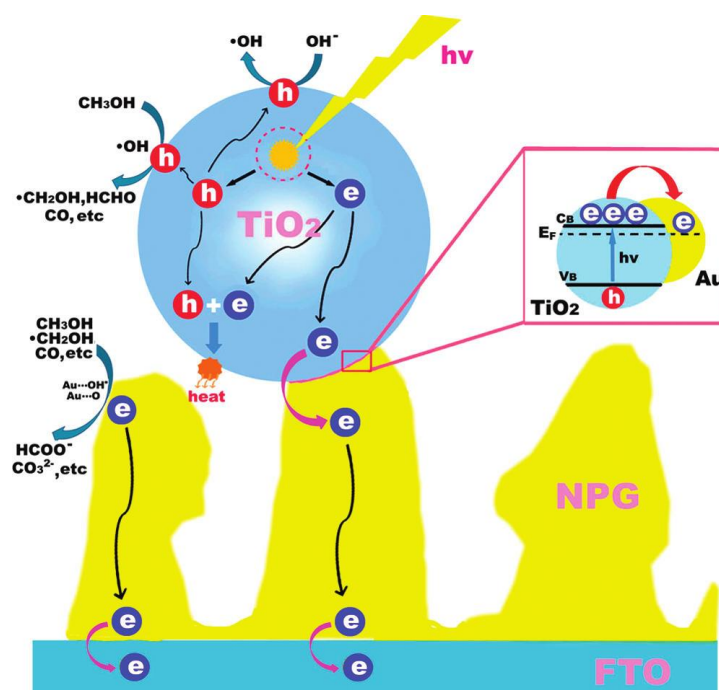


Figure 10

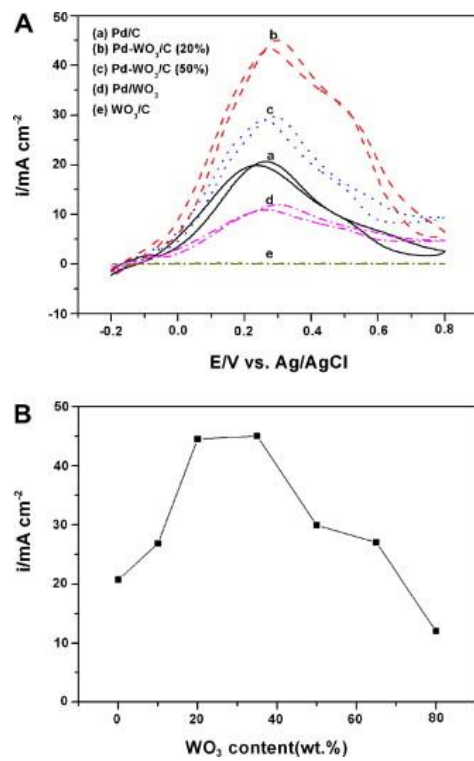


Figure 11

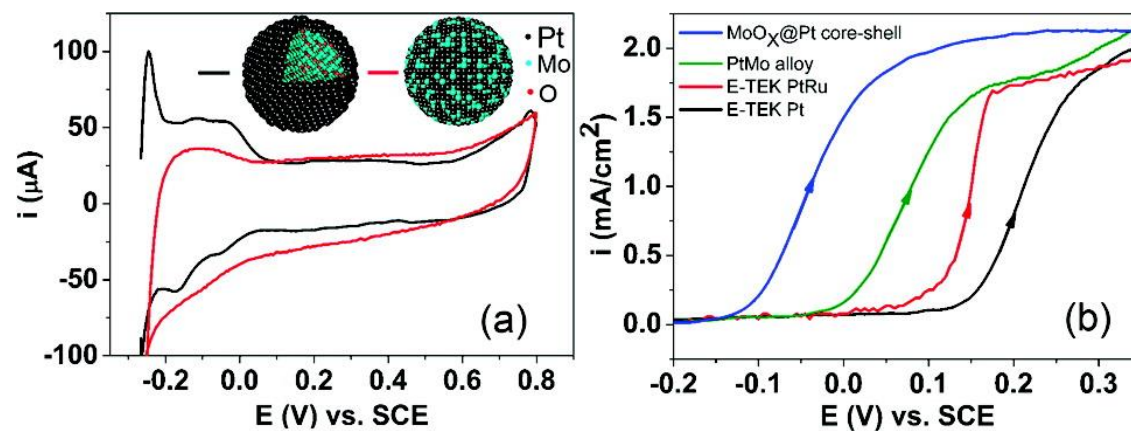


Figure 12

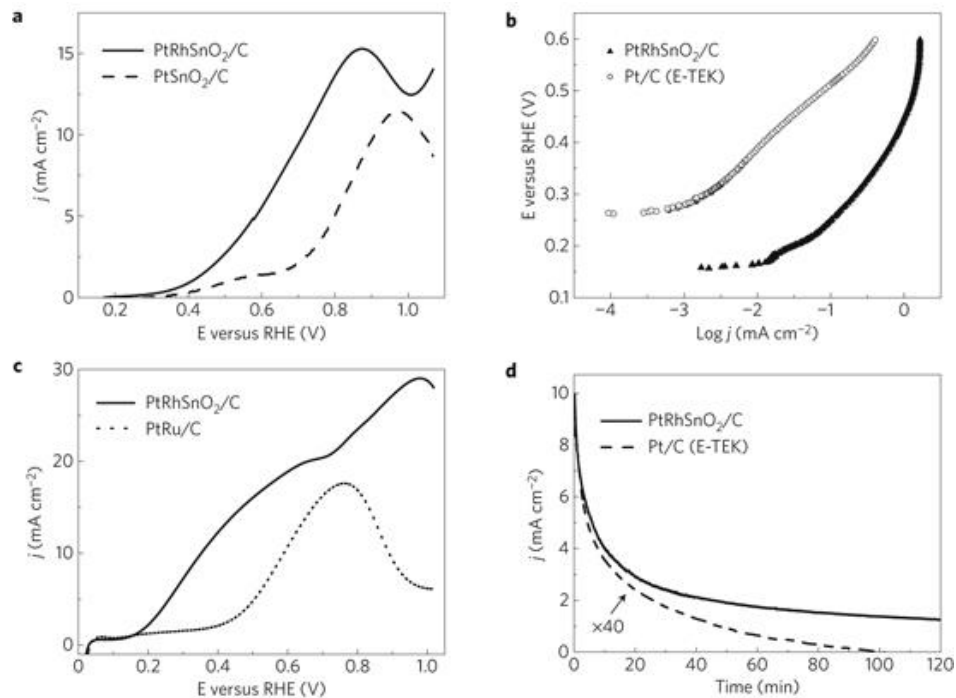


Figure 13

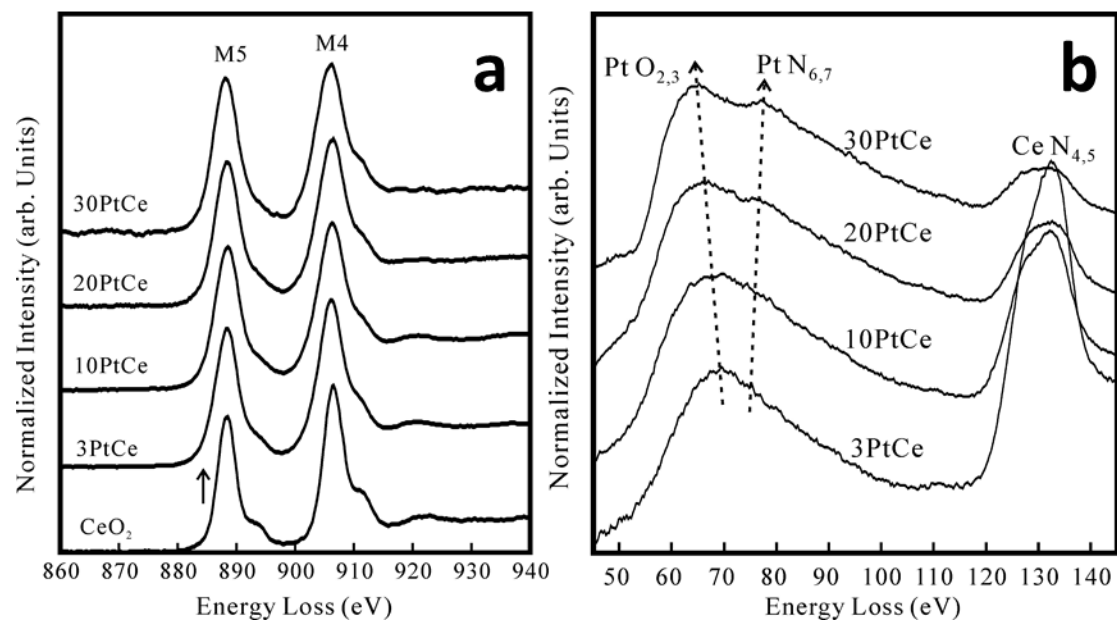


Figure 14

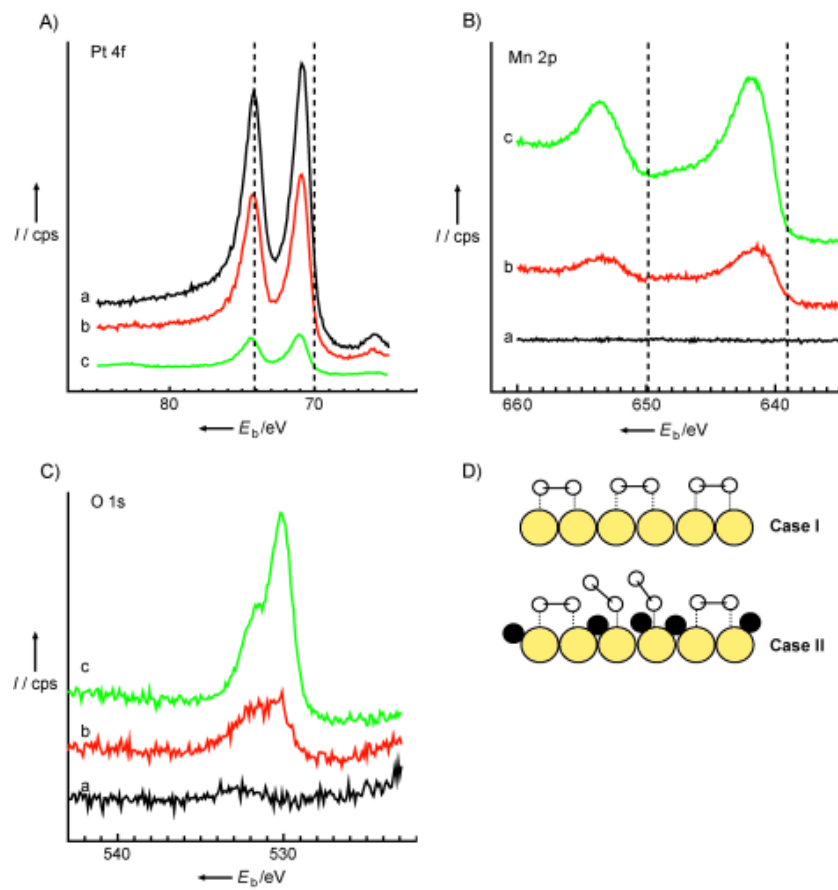


Figure 15

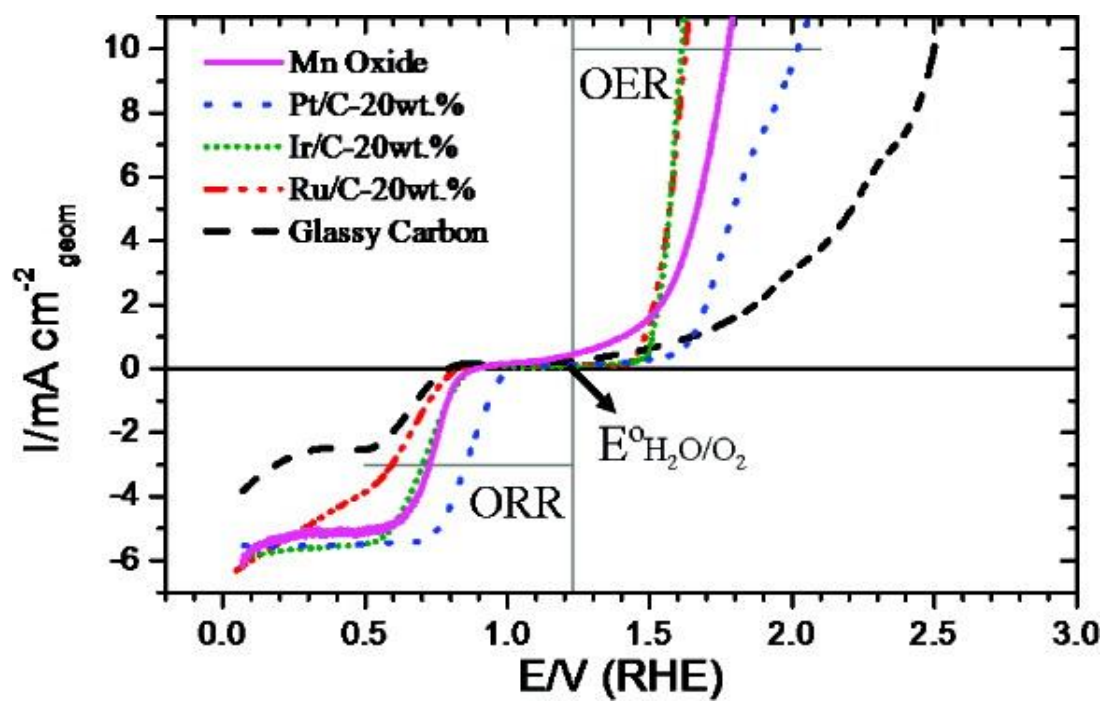


Figure 16

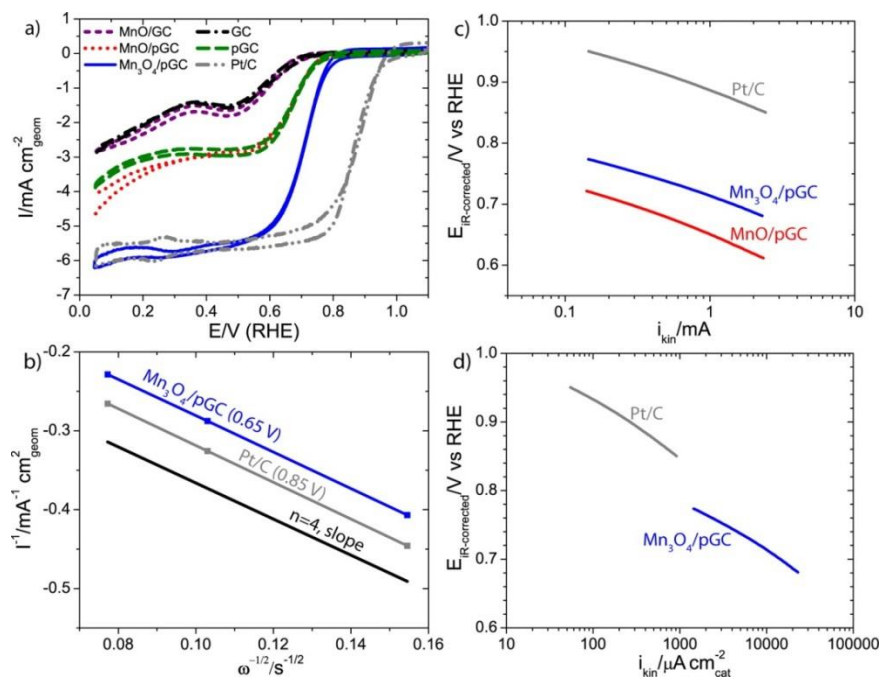


Figure 17

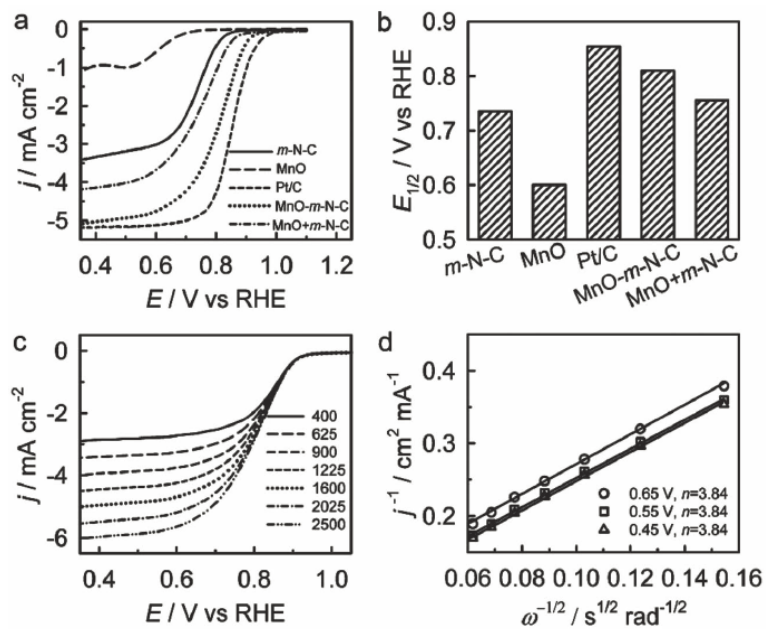


Figure 18

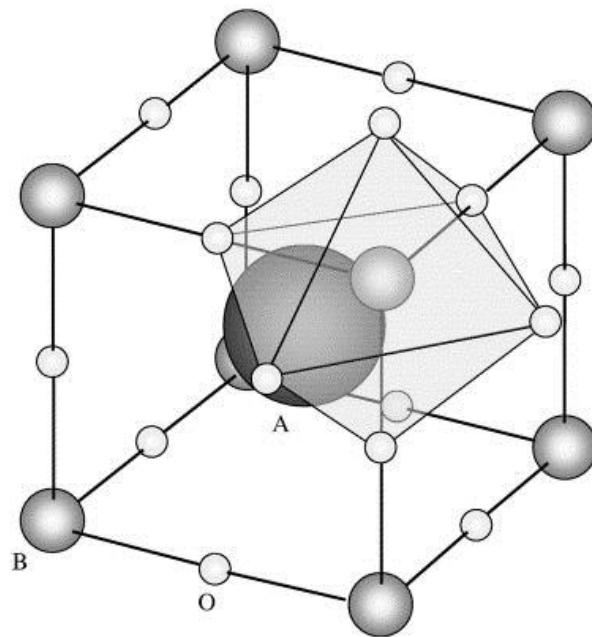
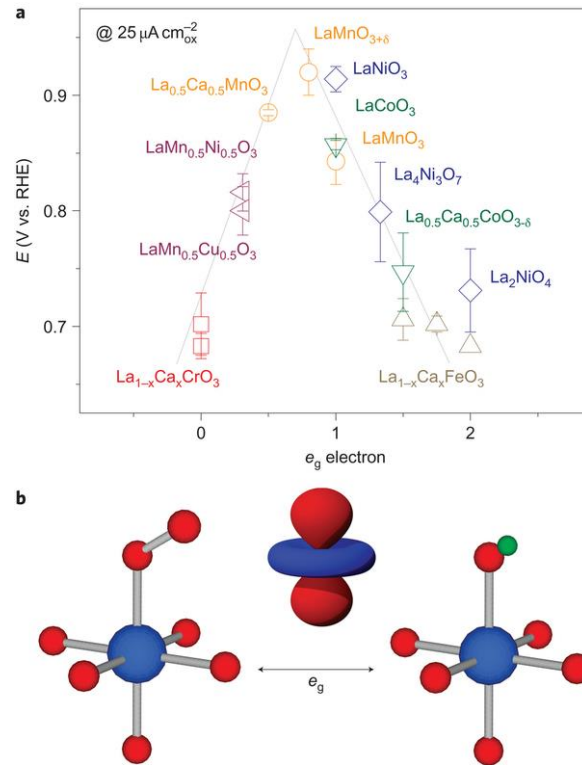


Figure 19



The table of contents entry:

Polymer electrolyte fuel cells (PEFCs) are promising power sources in portable and transportation applications because of their high-energy density, low-operating temperature and easiness in transportation and storage. However, high cost, low activity and short durability of electrocatalysts are restraining the commercialization of PEFCs. Metal oxides have abundant sources, low price, high chemical and electrochemical stability, abundant hydroxyl groups on the surface, and strong interaction with metal nanoparticles, and thus are promising to reduce the present problems in PEFCs. In this review, binary metal oxides such as titanium oxide, tungsten oxide, molybdenum oxide, ruthenium oxide, tin oxide, cerium oxide and manganese oxide, and multi-component perovskite oxides are chosen based on the selection criteria of metal oxides and introduced as independent electrocatalysts, co-catalysts and supports for various anode oxidation and cathode reduction reactions in PEFCs. The effects of compositions, morphologies, doping and mixing of metal oxides on their electrocatalytic performance for PEFCs have also been summarized. Finally, several most promising metal oxides and possible research trends on metal oxides are recommended for future PEFCs.